Master Thesis

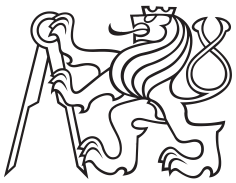

Czech Technical University in Prague

F4

Faculty of Nuclear Sciences and Physical Engineering
Department of Physics

Electron beam isochronous, achromatic focusing system: design and optimization

Bc. Pavel Gajdoš

Supervisor: Ing. Miroslav Krůs, PhD.
Field of study: Experimental Nuclear and Particle Physics
May 2019

Acknowledgements

I would like to sincerely thank my supervisor, Ing. Miroslav Krůs, Ph.D., for his willingness, patience and professsional feedback during the realization of this work.

Declaration

Prohlašuji, že jsem svou diplomovou práci vypracoval samostatně a použil jsem pouze podklady (literaturu, projekty, SW atd...) uvedené v přiloženém seznamu.

Nemám závažný důvod proti použití tohoto školního díla ve smyslu § 60 Zákona č. 121/2000 Sb., o právu autorském, o právech souvisejících správem autorským a o změně některých zákonů (autorský zákon).

V Praze dne 6. 5. 2019.

Abstract

The electron bunches accelerated by laser wakefield acceleration can reach a high energy and an ultrashort duration. This makes them a good candidate for applications, which desire a subpicosecond electron pulses. On the other hand, the energy spread of this beam is relatively large. Hence, if the beam propagates a long distance in the space its duration increases. To use such bunches for these application, they need to be compressed back. In this thesis, the scheme of electron beam achromatic, isochronous focusing system is proposed; such a system is capable to compress the bunch down to 600 fs as shown by SIMION numerical simulation. The acceptance of our focusing system should be more than 10 % of the beam energy, which was performed in simulations.

Keywords: achromatic, isochronous focusation; electron beam; laser wakefield acceleration

Supervisor: Ing. Miroslav Krůs, PhD.
Ústav fyziky plazmatu AV ČR, v. v. i.,
Za Slovankou 1782/3,
Praha 8

Abstrakt

Elektronové svazky urychlené laserem řízenou plazmovou vlnou mohou dosahovat vysokých energiích a ultrakrátkých délek. To z nich dělá vhodné kandidáty pro aplikace vyžadující subpikosekundové elektronové impulzy. Na druhé straně mají tyto svazky relativně velký rozptyl energie. A proto, pokud se svazek šíří po dlouhé vzdálenosti, jeho délka se prodlouží. Aby se daly takové svazky použít v těchto aplikacích, je nutné je komprimovat zpátky. V této práci je navrhnuto schéma achromatické, izochronní fokusující soustavy elektronového svazku; tento systém je schopen komprimovat svazek na 600 fs, jak je ukázáno numerickou simulací v programu SIMION. Akceptance fokusační soustavy by měla být více než 10 % energie svazku, což bylo ukázáno v simulacích.

Klíčová slova: achromatická, izochronní fokusace; elektronový svazek; laserové urychlování plazmovou vlnou

Překlad názvu: Návrh a optimalizace izochronní, achromatické fokusující soustavy elektronových svazků

Contents

Figures

Tables

Introduction

Nowadays, laser facilities with high power laser systems are able to generate stable, high energy electron bunches in a short distance. These bunches, produced by femtoseconds lasers, are also ultrashort with duration in the order of femtoseconds. Such ultrashort electron bunches are desired in various applications.

However, the electron bunches commonly accelerated by LWFA possess a relatively large energy spread. Hence, after propagation in the space their duration may be significantly prolonged. Therefore, the focusing system, that compresses the beam back, is required. Due to the not negligible energy spread the focusing system must ensure both chromaticity and isochronous corrections.

The aim of this thesis is the proposal of an electron beam isochronous, achromatic focusing system design and its optimization to provide the beam transport from LWFA. The considered electron beams are taken to correspond to the real electron beams accelerated during LWFA campains in the Ti:Sapphire laboratory in PALS research centre.

In the first two chapters we describe the basis of the laser wakefield acceleration and electron optics.

The following chapter contains a Matlab simulation of the particle trajectory change after propagation in focusing elements using a thin lens approximation.

The spatial chirp of the beam by dipole magnet is shown in the next chapter, where SIMION simulation is used to find out the correct dipole magnetic field and the distance between dipoles to obtain the required beam size.

Then, the initial scheme of the electron beam achromatic focusing system is proposed. Another simulation is used to determine the required sextupole field strength for the achromatic focusation.

The last chapter deals with an isochronous correction. The proposed scheme of achromatic, isochronous focusing system is shown. The simulation is provided to determine the beam duration in the focal spot.

Chapter 1

Laser wakefield acceleration

The concept of the particle acceleration in a plasma wave was firstly proposed 40 years ago [1]. Since then, laser-driven plasma-based accelerators have been of a great interest for the particle acceleration because they can accelerate particles to high energies in a short distance.

The laser wakefield acceleration uses the conversion of a transverse electric field of laser pulse into the longitudinal electric field of the plasma wave, i.e. creation of the wakefield via so-called ponderomotive force (see Sec. 1.1.1).

In comparision to convetional radio-frequency accelerators, the plasma-based accelerators can sustain much larger acceleration gradients. These gradients are limited in the conventional accelerators, typically ≈ 100 MV/m. The limitation is mostly due to electric breakdown of a material in acceleration cavities. Whereas the plasma waves can sustain a high electric field intensity in excess of

$$E_0(\mathrm{V/m}) \simeq 96\sqrt{n_0(\mathrm{cm}^{-3})}, \tag{1.1}$$

where n_0 is the plasma electron density in plasma. The relation (1.1) is valid only for linear plasma waves. More precisely $E_0 = cm_e\omega_p/e$, where m_e is electron mass, e electron charge and ω_p is the plasma frequency of electrons given by

$$\omega_p = \sqrt{\frac{n_0 e^2}{m_e \epsilon_0}}, \tag{1.2}$$

where ϵ_0 is the permitivity of vacuum. Using (1.1) and the electron plasma density $n_0 = 10^{18}$ cm^{-3}, the acceleration gradient in the plasma waves can reach 96 GV/m, which is three orders of magnitude greater than that of the conventional accelerators.

The plasma-based accelerators can produce ultra-short electron bunches. The plasma-wave wavelength is given

$$\lambda_p = \frac{2\pi c}{\omega_p}. \tag{1.3}$$

This implies, that the duration of accelerated electron bunch could be in the order of femtoseconds.

1.1 Plasma wave

The laser interaction with the plasma can be either linear or nonlinear. This depends on a normalized vector potetntial magnitude of the laser field

$$\vec{a} = \frac{e\vec{A}}{m_e c^2}, \tag{1.4}$$

which physically means the normalized transverse quiver momentum of a plasma electron in the laser field.

The peak amplitude a_0 of (1.4) is called the laser strength parameter, which can be calculated from the peak laser intensity I_0 as

$$a_0^2 = 7.3 \times 10^{-19} \left[\lambda(\mu\text{m})\right]^2 I_0 \left(\text{W/cm}^2\right), \tag{1.5}$$

where $\lambda = 2\pi/k$ is the laser wavelength and wave number k is defined through the laser frequency in vacuum $\omega = ck$.

The electron quiver motion is relativistic when $a_0 \geq 1$ and the laser-plasma interaction is nonlinear. This requires intensities $I \geq 10^{18}$ W/cm^2 for wavelengths $\lambda \simeq 1$ μm.

Analytical solutions for calculation of the plasma wakefields have been achieved only in 3D linear regime and 1D nonlinear regime. In 3D nonlinear regime numerical methods has to be used, as particle-in-cell.

The important parameter of the plasma wave is its phase velocity, by which several parameters are determined such as the minimum energy for electron trapping, the maximum energy gain, the maximum plasma wave amplitude and the dephasing length.

The plasma phase velocity is equal to a group velocity of the laser pulse, which excites the plasma wave[1]. The laser group velocity can be obtained from 1D dispersion relation

$$\omega^2 = c^2 k^2 + \omega_p^2, \tag{1.6}$$

where $\omega_p = ck_p$ is a plasma frequency. Therefore, the laser group velocity is

$$v_{g,L} = \frac{d\omega}{dk} = c\sqrt{1 - \frac{\omega_p^2}{\omega^2}} \tag{1.7}$$

and the Lorentz gamma factor has simple form $\gamma_{g_L} = \left(1 - v_g^2/c^2\right)^{-1/2} = \omega/\omega_p$. Nevertheless, the laser pulse group velocity is reduced by 3D effects, such as Rayleigh diffraction. Hence, the plasma phase velocity can be also affected. In the nonlinear regime, the group velocity corrections have to be provided as well. Both corrections can be found in [2].

[1] if the pulse evolution after its propagation is neglected

1.1.1 Ponderomotive force

The ponderomotive force is responsible for the creation of a wakefield. Since the ponderomotive force affets only plasma electrons (ions are too heavy to be influenced by commonly used ponderomotive force), the wakefield is produced by ejection of plasma electrons around the laser pulse envelope. For the linear 3D plasma waves the ponderomotive force can be calculated as

$$\vec{F}_p = -m_e c^2 \vec{\nabla}(a^2/2), \tag{1.8}$$

where $\vec{a}$ is a normalized vector potential of the laser field (1.4). Hence, the ponderomotive force is a gradient of the electromagnetic intensity or it could be viewed as a radiation pressure.

In the general nonlinear regime, the expression of the nonlinear ponderomotive force is

$$\vec{F}_{pN} = -m_e c^2 \vec{\nabla}\gamma \tag{1.9}$$

where γ is given by $\gamma = (1 + p^2)^{1/2}$ and $\vec{p}$ is electron momentum normalized to $m_e c$.

1.1.2 Wave breaking

Another important phenomenon in the plasma acceleration is wave breaking. As mentioned earlier, the plasma can sustain high electric fields of the plasma waves. The maximum amplitude in the linear regime can be determined from the Poisson equation

$$\vec{\nabla} \cdot \vec{E} = \frac{e}{\epsilon_0} (n_0 - n_e) \tag{1.10}$$

with the plasma wave electric field

$$E_z = E_{\max} \sin \left[\omega_p \left(\frac{z}{v_p} - t \right) \right] \tag{1.11}$$

and the cold nonrelativistic wave breaking field can be expressed as $E_{\max} = E_0 = c m_e \omega_p / e$.

However, the maximum value E_0 can be exceeded in the nonlinear regime. For the nonlinear plasma wave the maximum amplitude is [3]

$$E_{WB} = \sqrt{2} \, (\gamma_p - 1)^{1/2} \, E_0, \tag{1.12}$$

where, $\gamma_p = \left(1 - v_p^2/c^2\right)^{-1/2}$ and v_p is the phase velocity of the plasma wave, which is in the 1D limit (see Sec. 1.1) $\gamma_p \simeq \omega/\omega_p$.

The field E_{WB} is called the cold relativistic wave breaking field. When the amplitude of the plasma wave exceeds E_{WB}, the cold fluid equations are no longer valid and the warm fluid model has to be applied. The thermal effects in a warm plasma leads to a reduction of the plasma wave amplitude. Moreover, when E_{WB} is exceeded, electrons can be injected into the plasma wave by slipping into its acceleration phase. This will also reduce the plasma wave amplitude.

1.2 Electron acceleration

1.2.1 Limits of acceleration and energy gain

One of the limitating factors in the laser acceleration is a dephasing length. When an electron is accelerated in the plasma wave, propagating in z axis and the electric field described by

$$E(z) = E_{\max} \sin\left[\omega_p \left(\frac{z}{v_p} - t\right)\right], \tag{1.13}$$

an electron velocity is steadily icreasing and approaches the speed of light, $v_z \to c$. However, the phase velocity of the plasma wave is constant and smaller than the speed of light, $v_p < c$. Thus, it may be possible for the electron velocity to exceed the plasma phase velocity, $v_z > c_p$. After that, the electron eventually outrun the plasma wave and occurs in a decelerating phase, which means that its velocity is decreasing. Hence, the electron energy gain is limited. This is refered to as electron dephasing. The length, after which electron approaches the decelerating phase, ie. after which the electron phase slips by one half of a period of the plasma wave, is called dephasing length L_d. When the electron is highly relativistic ($v_z \simeq c$), the dephasing length is given by

$$\left(1 - \frac{v_p}{c}\right) L_d = \frac{\lambda_p}{2}. \tag{1.14}$$

The relation for L_d can be simplifed to $L_d \simeq \gamma_p^2 \lambda_p$, when $\gamma_p = \omega/\omega_p \gg 1$ is assumed.

The maximum energy gain W_{max}, which the electron can obtain after travelling the dephasing length, is roughly

$$W_{\max} \simeq eE_{\max} L_d \simeq 2\pi\gamma_p^2 \left(E_{\max}/E_0\right) m_e c^2, \tag{1.15}$$

assuming $E_{\max} < E_0$.

Considering the linear regime and 1D plasma waves, the electron acceleration can be studied by the electron position in a phase space $(\tilde{p}, \psi)$, where $\tilde{p}$ is the normalized momentum of electron and ψ is the phase of the plasma wave electrostatic potential given by

$$\phi = \phi_o \cos\psi = \frac{E_{\max}}{E_0} \cos\left[k_p \left(z - v_p t\right)\right], \tag{1.16}$$

The accelerating phase corresponds to the phase region $-\pi < \psi < 0$. The decelerating phase region is $0 < \psi < \pi$. If an electron would be accelerated it must have a sufficient initial energy. When it is injected at the phase ϕ and its initial velocity in a direction of the wave propagation z is smaller than the plasma phase velocity $v_z < v_p$, the electron is slipping backwards through the plasma wave. Therefore, if the initial electron velocity is not sufficient, the electron could not gain enough energy and its velocity at phase $\psi = -\pi$ would be still $v_z < v_p$, which means that it will be untrapped and will be

moving to the opposite direction with respect to the plasma wave. On the other hand, when the electron's initial velocity is high, such that $v_z > v_p$ at phase $\psi = -\pi$, the electron becomes trapped and it will orbit at $-\pi < \psi < \phi$.

Another limitation of the energy gain in the laser plasma acceleration is due to a pump depletion. When the laser pulse creates the plasma wave, it looses its energy (the pump depletes). The length, after which the laser pulse does not have enough energy to create the plasma wave and also it cannot be self-guided, is called a pump-depletion length L_{pd}. In the linear regime, the dephasing length is much smaller than the pump depletion length ($L_d \ll L_{pd}$, thus the energy gain is limited only by L_d. There are several methods, by which the dephasing length can be extended. One of them is tapering of the density of plasma in the direction of its propagation. If the plasma density is smaller the wavelength of the plasma wave is longer, which increases the plasma wave phase velocity. After that, the acceleration will be limited by the pump depletion length

$$L_{pd} \sim \frac{\lambda_p^2}{\lambda^2} a_0^{-2}, \tag{1.17}$$

where λ_p and λ are wavelengths of the plasma wave and the laser pulse, repectively.

In the nonlinear regime the pump depletion length is similar to the dephasing length $L_{pd} \sim L_d$. Thus, no density tapering is needed because the energy gain is limited by the pump depletion length.

The energy gain can also be limited by Rayleigh diffraction. The laser spot size radius evolves[2](considering the propagation in z axis) as

$$r_s(z) = r_0 \sqrt{1 + \frac{z^2}{Z_R^2}}, \tag{1.18}$$

where r_0 is the spot size at the focal point $z = 0$, given by Rayleigh length Z_R by the relation

$$Z_R = \frac{k r_0^2}{2}, \tag{1.19}$$

where k is a wave number. If the laser beam is not optically guided in the plasma, the interaction length of the laser pulse and the plasma wave will be limited to several Rayleigh lengths. Hence, the laser acceleration to high energies would not be possible in such a plasma wave. Nevertheless, the laser beam can be guided using various methods, one of them is described in Sec. 1.2.2.

As mentioned above, the energy gain is limited by several mechanisms. In LWFA it can be estimated using

$$\Delta W = e E_z L_{acc} \tag{1.20}$$

where L_{acc} is the acceleration length and $E_z = E_0 (a_0^2/2)(1 + a_0^2/2)^{-1/2}$ is driven by a flat-top, linearly polarized laser pulse. Here we show the energy

[2]in the paraxial approximation

gain in practical units for all three limitating cases neglecting the self guiding and plasma instabilities. For the acceleration length limited by Rayleigh diffraction $L_{acc} \simeq \pi Z_R < L_d, L_{pd}$ [4], the energy gain is

$$\Delta W_R\,(\mathrm{MeV}) \simeq 740 \left(\frac{\lambda}{\lambda_p}\right) \left(1 + \frac{a_0^2}{2}\right)^{-1/2} P\,(\mathrm{TW})\,. \tag{1.21}$$

When L_{acc} is limited by the dephasing length ($L_{acc} \simeq L_d$), the energy gain is

$$\Delta W_d\,(\mathrm{MeV}) \simeq \frac{630 I\left(\mathrm{W/cm^2}\right)}{n\,(\mathrm{cm^{-3}})} \times \begin{cases} 1, & a_0^2 \ll 1 \\ (2/\pi)/N_p, & a_0^2 \gg 1, \end{cases} \tag{1.22}$$

where N_p is the number of plasma periods behind the wave driving laser pulse. In case of the limitation by the pump depletion ($L_{acc} \simeq L_{pd}$), the energy gain is

$$\Delta W_{pd}\,(\mathrm{MeV}) \simeq \begin{cases} 3.4 \times 10^{21} / \left[\lambda^2\,(\mu\mathrm{m})\, n\,(\mathrm{cm^{-3}})\right], & a_0^2 \ll 1 \\ 400 I\left(\mathrm{W/cm^2}\right), & a_0^2 \gg 1. \end{cases} \tag{1.23}$$

1.2.2 Self-guiding

Considering a high intensity laser beam propagating through the underdense plasma, the refractive index of the plasma is given by (assuming 1D limit and small amplitudes of laser beam propagating through homogenous plasma)

$$\eta = \sqrt{1 - \frac{\omega_p^2}{\omega^2}}. \tag{1.24}$$

The relativistic mass of electrons is increased when the laser pulse is interacting with them. Moreover, the ponderomotive force expells the electron radially from the centre of the laser pulse. Thus, the plasma density is small near the propagation axis and it is getting higher in the radial direction from the propagation axis, i.e. in the centre of the laser pulse the plasma frequency gets smaller which (by (1.24)) increases plasma refractive index η. Therefore, the medium behaves as a convex lens.

The laser pulse is self-guided when the laser power exceeds a critical value [5] given by

$$P_{cr} \simeq 17.4 \left(\frac{\omega}{\omega_p}\right)^2 \mathrm{GW}. \tag{1.25}$$

1.3 Electron injection

The injecton of electrons into the plasma wave is the cruicial part of a laser acceleration. The injection affects properties of the accelerated electron beams, such as charge, energy, energy spread, etc. In this section, several methods of acceleration will be discussed.

1.3.1 Self-injection

The simpliest way to inject electrons into the accelatio phase is so-called self-injection, by which electrons are injected into the plasma wave by itself. The self-injection may also accompany other injection mechanisms. The electron bunch injected by this method has usually a high charge (up to 10 nC) but also a large energy spread. As mentioned in Sec. 1.1.2 (1D limit and cold plasma) the self-injection occurs when the plasma wave amplitude exceeds the wave breaking limit given by (1.12). However, experimentally measured plasma wave amplitudes are smaller, the effective amplitudes are in the range $E_z/E_0 \sim 10 - 30\%$. Even if 3D and thermal effects are counted in, the wave breaking amplitude is still higher than E_0. Thus, some other plasma instabilities (e.g. Ramman backscattering) must be present to lower the wave breaking amplitude and enable self-injection.

There are two main reasons which causes a large energy spread of the accelerated electron bunch. Firstly, electrons are trapped by the self-injection during the whole path of the laser propagation in the plasma. Therefore, the electrons injected near the end of the path gain less energy than others. Secondly, the dephasing length is typically smaller than the distance in which the laser travel in the plasma. Hence, the electrons are permanently accelerated and decelerated in the plasma wave depending on which part they are situated in. The maximum energy of the electrons trapped by the self-injection is

$$W_{\max} \simeq 4\gamma_p m_e c^2 \frac{E_z}{E_0}, \tag{1.26}$$

if $E_z/E_0 \ll 1$. Nevertheless, the self-injection is very unstable due its general nonlinear nature. Thus, other more stable and controlled mechanisms are being developed.

1.3.2 Ionization injection

Other method is the ionization injection, which occurs even with lower intensities of the laser pulse. The ionization injection is also very simple with respect to other mechanisms. Furthermore, monoenergetic electron beams can be produced by this method.

The basis of this mechanism is the use of a large energy difference between energy levels in an atomic shell. Usually, a gas mixture, which contains one element with low atomic number and other element with the higher atomic number, is used. For example, the ionization energy of the electron in the helium K-shell and nitrogen L-shell are in the range from 10 eV to 100 eV, but the ionization energy for the first and the second electron in the nitrogen K-shell is 550 eV and 670 eV, respectively. Thus, when the laser pulse interacts with the gas mixture, the electrons in the helium K-shell and nitrogen L-shell are ionized by the leading edge of the laser pulse, creating the plasma wave. Whereas, the electrons in the nitrogen K-shell are ionized around the peak intensity of the pulse, hence, inside the plasma wave. If these electrons are located in accelerating region, they are trapped.

1.3.3 Density transition

The electrons can be also trapped at the transition between plasmas with different densities if the transition length L_{tr} is long compared to wavelength λ_p of the plasma wave [6]. However, the sharp density downramp is desirable because it is used to generate monoenergetic electron beams [7]. The plasma wave has to propagate from the plasma with higher density to the less dense plasma. At the transition, the plasma wavelength is getting longer and the phase velocity of the plasma wave is decreasing. The plasma wave has the form

$$\phi = \phi_0 \cos k_p \zeta = \phi_0 \cos k_p \left(z - ct\right). \tag{1.27}$$

Consider the position of the phase peak N_p periods behind the drive pulse. The positions of the phase peak are $\mid \zeta_1 \mid = N_p \lambda_{p1}$ before transition and $\mid \zeta_2 \mid = N_p \lambda_{p2}$ after transition. The plasma wavelengths $\lambda_{p1,2}$ depends on the plasma densities $n_{1,2}$ such that $\lambda_{p1} < \lambda_{p2}$ for $n_1 > n_2$. Hence, after the transition, the position of the phase peak is shifted by

$$\Delta \left|\zeta\right| = N_p \left(\lambda_{p1} - \lambda_{p2}\right) \tag{1.28}$$

and the phase velocity of the plasma wave is changed by

$$\frac{\Delta v_p}{c} \simeq \frac{N_p \left(\lambda_{p1} - \lambda_{p2}\right)}{L_{tr}}. \tag{1.29}$$

Thus, the change of the phase velocity is proportional to the change of the magnitude of the plasma density. The local phase velocity of the plasma wave (assuming small variation of the phase velocity) is

$$\frac{v_p}{c} - 1 \simeq -\frac{\zeta}{k_p}\frac{dk_p}{dz} = -\frac{\zeta}{2n}\frac{dn}{dz}. \tag{1.30}$$

The phase ζ is negative because it takes place behind the pulse. Therefore, the local phase velocity of plasma wave decreases for decreasing density ($dn/dz < 0$).

The electrons are trapped when the wake local phase velocity is equal to the velocity of electrons oscilating in the plasma $v_p = v_e$. Since v_p decreases for the decreasing density, the electron injection occurs at some point of the transition.

1.3.4 Optical injection

Since the plasma wave is driven by femtosecond laser pulses, it is very challenging to use electrical devices as electron injectors, which work in nanosecond timescale[3]. However, the femtosecond timing of multiple high-intensity laser pulses can be achieved easily. Thus, the electrons can be

[3] however, photocathodes driven by fs laser pulses can be used for generation of fs electron bunches

injected into the plasma wave period optically using multiple ultrashort high-intensity laser pulses. Two main geometries are used for the optical injection. Either the drive pulse and injection pulse(s) propagate parallel or perpendicular to each other.

The electron bunches with a low energy spread ($< 10\%$) can be produced when two high-intensity laser pulses propagating perpendicularly to each other are used. The first drive pulse generate the plasma wave and the second injection pulse crosses the plasma wave at certain distance behind the drive pulse [8]. The injection occurs due to the ponderomotive force of the injection pulse, which accelerates some plasma electrons so they are trapped in a plasma wakefield. The focal spot size and the pulse length of the injection has to be small compared to the wavelength of the plasma wave to inject electrons into a single plasma wave period.

In other method (with similar geometry), two laser pulses are also used but the injection pulse intensity is much lower and pulses has perpendicular polarization to one another. Moreover, these two pulses has to intersect in the same focal spot at the same time. Numerical simulations [9] show the injection of the high energy electron bunch and a low energy spread when the intensity of the injection pulse is 1% of the drive pulse intensity.

Two or three laser pulses can be used to achieve an injection in a parallel geometry. In the more simple two pulse scheme the drive and injection pulse counterpropagate and have the same polarization. The tail of the drive pulse beats the injection pulse creating a standing wave, which causes dephasing of the electrons and they become trapped. Practically, the laser pulses are collided at an angle to prevent the damage of the laser system. In the three pulse scheme two injection pulses are used. One of them propagates forward behind the drive pulse and the other propagates backwards. Both injection pulses has orthogonal polarization with respect to the drive pulse, so the backward pulse does not beat the drive pulse. The two injection pulses interact behind the drive pulse and create a pondermotive beat wave, which can trap plasma electrons and they can be injected into the stronger plasma wave created by the drive pulse.

Chapter 2

Electron optics

The beam transport system is a significant part of any accelerator. Its role is to guide the beam along the predefined path and change the size of the beam (or keep the same) as needed. The system consists of beam guidance and focusing systems. The change of the beam trajectory and focusing is usually provided by magnets via Lorentz force.

2.1 Particle motion in electromagnetic field

When a particle with the charge e moves in the electromagnetic field, the interacting Lorentz force is

$$\vec{F} = e\vec{E} + e\left(\vec{v} \times \vec{B}\right), \tag{2.1}$$

where $\vec{E}$, $\vec{B}$ and $\vec{v}$ are electrical and magnetic field vectors and the particle velocity vector, respectively. The beam dynamics is reffered to as an evolution of the beam trajectory, when the Lorentz force is applied. The Lorentz force depends on both electrical and magnetic fields. Assuming the relativistic particle ($v \approx c$), the Lorentz force generated by magnetic field of 1 T is the same as that produced by electric field of 300 MV/m. The generation of magnetic fields of 1 T can be done relatively easily. On the other hand, the generation of electrical field of 300 MV/m is very challenging. Thus, the beam focusing and guidance is mostly provided by magnetic fields. If the particle has a low velocity ($v \ll c$), the effectivness of magnetic factor is scaled with a particle velocity $\beta = v/c$.

2.1.1 Beam guidance

To change the trajectory of a charged particle, magnetic fields are used. The deflection can be determined by the equilibration of the Lorentz force and the centrifugal force

$$m\gamma v^2\vec{\kappa} + e\left(\vec{v} \times \vec{B}\right) = 0, \tag{2.2}$$

where γ is the relativstic Lorentz gamma factor and $\vec{\kappa} = (\kappa_x, \kappa_y, 0)$ is the local curvature vector of the trajectory defined as

$$\kappa_{x,y} = \frac{1}{\rho_{x,y}} \tag{2.3}$$

and $\rho_{x,y}$ is the local curvature radius of the particle trajectory.

To simplify the calculation, lets assume, that the magnetic field vector $\vec{B}$ is oriented perpendicularly to the velocity vector $\vec{v}$ of the charged particle propagating in the z axis. Moreover, transversal velocities $v_{x,y}$ are neglected, because they are too small compared to v_z for relativistic particle. The curvature radius of the particle trajectory can be expressed (taking particle momentum $p = m\gamma v$) as

$$\frac{1}{\rho} = \left|\frac{e}{p}B\right| = \left|\frac{ec}{\beta E}B\right|, \tag{2.4}$$

where E is the energy of the particle. The beam rigidity is defined as

$$|B\rho| = \frac{p}{e} \tag{2.5}$$

and it is used for normalization of the magnet strength. In practical units the beam rigidity and curvature is

$$|B\rho|\,(\mathrm{Tm}) = \frac{10}{2.998}\beta E\,(\mathrm{GeV}) \tag{2.6}$$

and

$$\frac{1}{\rho}\left(\mathrm{m}^{-1}\right) = 0.2998\frac{|B\,(\mathrm{T})|}{\beta E\,(\mathrm{GeV})}, \tag{2.7}$$

respectively. These expressions become even more simple for relativistic particles since $\beta \approx 1$. For ions with a charge Ze and nucelon number A, the correction factor Z/A has to be added and $E\,(\mathrm{GeV/u})$ has to be evaluated as the total energy per nucleon.

2.2 Beam focusing

The concept of focusing of charged particles can be viewed in a similiar way as in the classical optics. Instead of glass lenses in photon optics, magnetic fields are used, which deflects the particle such that the angle of deflection α is proportional to distance r from the centre of the focusing device.

From Fig. 2.1 the deflection angle can be expressed as

$$\alpha = -\frac{r}{f}, \tag{2.8}$$

where r is the focal length of the lens. For charged particle beams the deflection angle can be obtain using the azimuthal magnetic field B_ϕ

$$\alpha = -\frac{l}{\rho} = -\frac{e}{\beta E}B_\phi l = -\frac{e}{\beta E}grl, \tag{2.9}$$

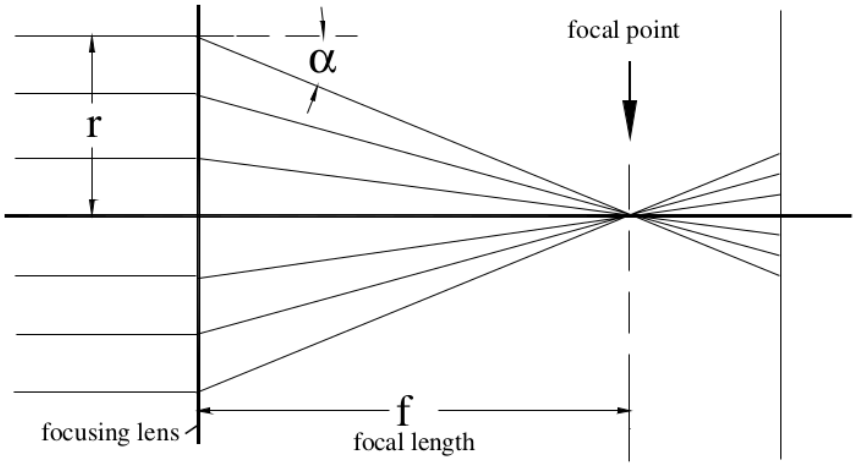

Figure 2.1: Focusing principle.

where l is the length which the particle travels in the magnetic field (magnet length) and g the gradient of the magnetic field defined as

$$g = \frac{dB_\phi}{dr}. \tag{2.10}$$

In (2.9) the length l is assumed to be very small compared to the focal length f in a way that the distance r is not changed significantly in the magnetic field.

There are two options to obtain the form of (2.8). Either the azimuthal magnetic field B_ϕ or the magnet length l has to be linearly dependent on the distance from the axis of the focusing device.

Although, it is possible to build magnets with lengths linearly dependent on r, it is easier to use the magnetic fields which are increasing linearly with r and keeping the magnet length l constant. One of the devices which fulfills these conditions is a quadrupole magnet. This magnet is mostly used to focus charged beams. The advantage, that quadrupole possesses over other possible magnets, is its free aperture, i.e. no part of the magnet (wires etc.) is in the beam trajectory.

The potential of quadrupole magnet is

$$V = -gxy, \tag{2.11}$$

hence the magnetic field in Cartesian coordinates is

$$-\frac{dV}{dx} = B_x = gy \tag{2.12}$$

$$-\frac{dV}{dy} = B_y = gx. \tag{2.13}$$

As mentioned, the magnetic field grows linearly from the optical axis. The equipotential lines of the quadrupole magnets are hyperbolas.

The focal length f of the magnet can be expressed using the focusing strength defined by

$$k = \frac{e}{p}g = \frac{ec}{\beta E}g. \tag{2.14}$$

From (2.9) the focal length is

$$f^{-1} = kl. \tag{2.15}$$

In practical units, the focusing strength can be obtained by

$$k\left(\mathrm{m}^{-2}\right) = 0.2998\frac{g\,(\mathrm{T/m})}{\beta E\,(\mathrm{GeV})}. \tag{2.16}$$

Similarly to the curvature radius (2.7), multiplication by Z/A is needed to obtain the focusing strength for ions.

Due to their magnetic fields, the quadrupoles are focusing in one plane and defocusing in the other. However, focusing in both planes can be achived when more quadrupoles are combined. Considering two quadrupoles with focal lengths f_1 and f_2 and the distance betwen them d, the total focal length of this system is given by

$$\frac{1}{f} = \frac{1}{f_1} + \frac{1}{f_2} - \frac{d}{f_1 f_2}. \tag{2.17}$$

In a special case, which satisfises $f_1 = -f_2$, the total focal length would be

$$\frac{1}{f} = \frac{d}{|f_1 f_2|}. \tag{2.18}$$

Thus, this system is focusing in both planes.

2.3 Beam transport

The general equations of motion are rather complicated and usually expressed by perturbative expansion [10]. If beam transport systems constist only of bending and quadrupole magnets, we can restrict to linear terms of equations of motions, which simplifies the solution. Such beam transport systems are called linear systems.

Assuming the bending of the beam only in x-plane (without restriction of generality), the magnetic fields can be written as

$$\begin{aligned} B_x &= -gy \\ B_y &= B_{y0} + gx, \end{aligned} \tag{2.19}$$

where B_{y0} is a magnetic field of the dipole magnet and g is a field gradient of quadrupole magnetic field. Then, the linear equations of motion are

$$\begin{aligned} x'' + (k_0 + \kappa_{0x})\, x &= 0 \\ y'' - k_0 x &= 0, \end{aligned} \tag{2.20}$$

where k_0 is the focusing strength of quadrupole and κ_0 is a bending term associated with the dipole magnet.

The focusing from both dipole and quadrupole can be combined into one strength parameter

$$K(z) = k_0(z) + \kappa_{0x}^2(z). \tag{2.21}$$

If only one magnet (dipole or quadrupole) is used either $k_0(z)$ or $\kappa_{0x}^2(z)$ is zero. If both magnets are combined, then both terms are nonzero.

2.3.1 Matrix formalism

The solution to (2.20) can be expressed in a matrix formalism. For simplicity we use a so-callded hard edge model, which means that the focusing parameter $K(z)$ changes like a step function along the beam transport axis (it is zero outside the magnet and maximal inside). Thus, the beam transport axis can be cut into pieces where K is constant and the particle trajectory can be calculated separatly in each part.

If this is applied, equations of motion are the same as for the harmonic oscillator

$$u'' + Ku = 0, \quad \text{where} \quad K = k_0 + \kappa_{0x}^2(z) = \text{const} \tag{2.22}$$

and u can be taken as x or y. The principal solutions for $K > 0$ are

$$C(z) = \cos\left(\sqrt{K}z\right) \quad \text{and} \quad S(z) = \frac{1}{\sqrt{K}} \sin\left(\sqrt{K}z\right), \tag{2.23}$$

and for $K < 0$

$$C(z) = \cosh\left(\sqrt{|K|}z\right) \quad \text{and} \quad S(z) = \frac{1}{|K|} \sinh\left(\sqrt{|K|}z\right). \tag{2.24}$$

Any arbitrary solution can be formed by the linear combination of these two principal solutions

$$\begin{aligned} u(z) &= C(z)u_0 + S(z)u_0 \\ u'(z) &= C'(z)u_0' + S'(z)u_0'. \end{aligned} \tag{2.25}$$

The u_0 and u_0 are initial conditions of a particle trajectory, which can be also chosen arbitrary.

In the matrix formalism the solution to (2.22) can be expressed as

$$\begin{pmatrix} u\,(z) \\ u'\,(z) \end{pmatrix} = \begin{pmatrix} C_u(z) & S_u(z) \\ C_u'(z) & S_u'(z) \end{pmatrix} \begin{pmatrix} u\,(z_0) \\ u'\,(z_0) \end{pmatrix}. \tag{2.26}$$

2.3.2 Drift space

The evolution of the particle trajectory after travelling a drift space of the length $l = z - z_0$ (or a very weak magnet) is given by

$$\begin{pmatrix} u(z) \\ u'(z) \end{pmatrix} = \begin{pmatrix} 1 & l \\ 0 & 1 \end{pmatrix} \begin{pmatrix} u(z_0) \\ u'(z_0) \end{pmatrix} \tag{2.27}$$

This transformation matrix exhibits a desired feature, which is no change of the position of a particle with a zero slope $u'(z_0) = 0$, i.e. the collimated beam is not changed in a drift space.

2.3.3 Quadrupole magnets

For the quadrupole magnet the dipole term from (2.20) is zero and the field strength k can be both possitive and negative. Considering a particle entering a magnet at z_0, the solution of equations of motion in the matrix formalism for a particle at a point z is

$$\begin{pmatrix} u(z) \\ u'(z) \end{pmatrix} = \begin{pmatrix} \cos\psi & \frac{1}{\sqrt{k}}\sin\psi \\ -\sqrt{k}\sin\psi & \cos\psi \end{pmatrix} \begin{pmatrix} u(z_0) \\ u'(z_0) \end{pmatrix}, \tag{2.28}$$

where $\psi = \sqrt{|k|}\,(z - z_0)$. This is valid only if z_0 and z are in quadrupole magnetic field. For a defocusing quadrupole, where $k = -\sqrt{|k|}$, the similiar solution is

$$\begin{pmatrix} u(z) \\ u'(z) \end{pmatrix} = \begin{pmatrix} \cosh\psi & \frac{1}{|k|}\sinh\psi \\ \sqrt{|k|}\sinh\psi & \cosh\psi \end{pmatrix} \begin{pmatrix} u(z_0) \\ u'(z_0) \end{pmatrix} \tag{2.29}$$

The phase is $\psi = \sqrt{|k|}\,(z - z_0)$. To get a transformation matrices for a full length l of a quadrupole, we can set $l = z - z_0$ to (2.28) and (2.29.

2.3.4 Thin lens approximation

To simplify calculations, the thin lens approximation can be useful. Assume a thin quadrupole, such that its length is much smaller then the focal length. Therefore, $l \to 0$ and the phase $\phi = \sqrt{k}l \to 0$. The focal length remains constant

$$f^{-1} = kl = \text{const.} \tag{2.30}$$

The transformation matrices are simplified and have the same form in both planes with the exception of the sign of the focal length f

$$\begin{pmatrix} u(z) \\ u'(z) \end{pmatrix} = \begin{pmatrix} 1 & l \\ -\frac{1}{f} & 1 \end{pmatrix} \begin{pmatrix} u(z_0) \\ u'(z_0) \end{pmatrix}, \tag{2.31}$$

where

$$\begin{aligned} f^{-1} = kl > 0 \quad & \text{in the focusing plane} \\ f^{-1} = kl < 0 \quad & \text{in the defocusing plane.} \end{aligned} \tag{2.32}$$

2.4 Chromaticity corrections

The beam focusing with the quadrupole magnets works very well for monoenergetic beams. However, the focal spot broadens with the increasing energy spread of the beam. The correction can be provided by the sextupole magnets. These magnets have different magnetic profiles, which allow focusing in one half-plane and defocusing in the other. The correction comes from higher order terms of perturbative solution of equations of motion.

The scheme of the chromaticity correction using the sextupole magnet is shown in Figure 2.2. The beam has to be firstly spatially chirped, such that particles with higher energies are above the optical axis and vice versa. The sextupole focuses particles above the beam axis and defocuses particles under the beam axis. By finding the right magnetic field strength of the sextupole magnet, all particles can be focused in the one focal spot.

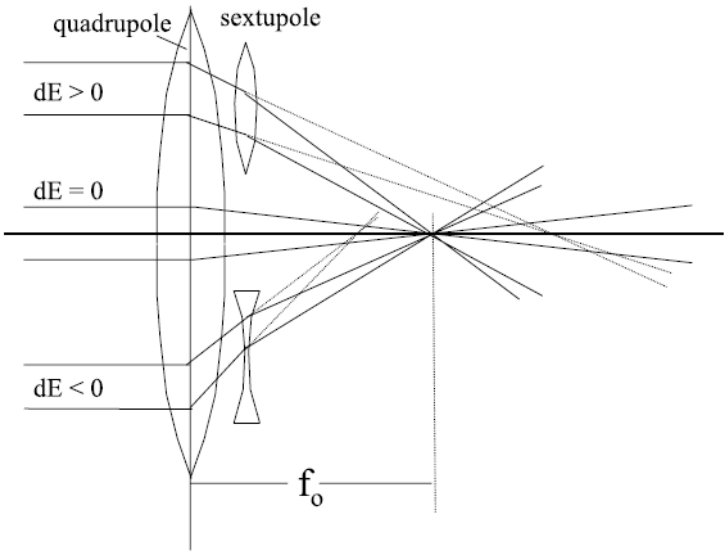

Figure 2.2: Achromatic correction using sextupole magnet.

2.5 Beam emittance and acceptance

One of the main paramaters, that determine the property of the beam, is called the beam emittance. It can be viewed as an area in phase space which is occupied by beam particles, i.e. emittance is the abillity of the beam to be focused and it describes the "size of the beam". In a phase space, the particle is characterized by its position and momentum in each axis. Therefore, there are two transversal and one longitudinal emittances. It is convenient to use the slope (x', y') of the particle instead of its momentum for high energy beams with $p_z \gg p_x, p_y$.

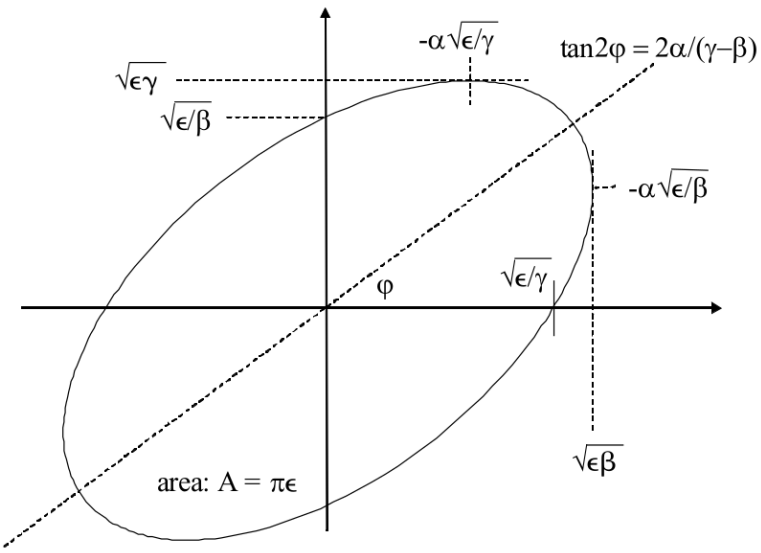

Figure 2.3: Phase space ellipse.

In the phase space, all particles of the beam can be surrounded by phase ellipse (see Fig. 2.3). Considering x-plane the phase ellipse is described by

$$\gamma x^2 + 2\alpha x x' + \beta x'^2 = \epsilon, \tag{2.33}$$

where γ, α, β are ellipse parameters describing its shape and orientation and ϵ is another ellipse parameter called emittance, which is defined by the area of the ellipse A as

$$A = \int_{\text{ellipse}} dx dx' = \pi\epsilon. \tag{2.34}$$

According to Liouville's theorem, the beam emittance is preserved during the propagation through any beam transport system. By choosing the particle with the largest phase ellipse, it is possible to determine the collective behaviour of the beam using a motion of a single particle because all other particles, that are located in that ellipse, will stay inside the ellipse.

As mentioned above, the beam emittance cannot be changed, only the shape of the phase ellipse. However, not all particles of the beam can be transported by the beam transport system (e.g. small aperture). The characteristic of the transport line, that shows which particle can be transported, is called acceptance, defined as the maximal emittance which can pass through the system.

Chapter 3

Sextupole field gradient determination using the thin lens approximatio

In this chapter, we show the estimated value of the magnetic field gradient of the sextupole to correct the focusation of the electron beam into one focal spot by two quadrupole magnets in one plane. To simplify calculations, the thin lens approximation is used. The electron beam parameters were taken arbitrary but consistent to the real ones. The caluculations of a particle trajectories were performed in Matlab.

Since this work aims at focusing of nonmonoenergetic electron beams and according to the commonly generated electron beam energy spreads during LWFA experiments in Ti:Sapphire laboratory at PALS, the energy range from 60 MeV to 110 MeV was chosen[1].

Suppose the electron beam propagating in z-axis separated by energy levels in x-axis. The beam diameter is 10 cm and its energy varies from 60 MeV to 110 MeV. Energy lines are distributed in a such way, that particle trajectories corresponding to the with higher energy than the mean value (85 MeV) are above the optical axis and lines with energy lower than 85 MeV are below it without loss of generality. Only lines with energies 60, 65, 70, 75, 80, 85, 90, 95, 100, 105, 110 MeV were chosen for the calculation of their trajectories. The distance between two neighboring lines was set to 1 cm starting with 110 MeV energy line at the position $x = 5\,\mathrm{cm}$.

Firstly, we will focus on the beam propagation through two quadrupoles only (focusing and defocusing). The thickness of both quadrupoles is set to $l = 1\,\mathrm{cm}$. The distance of the drift space between quadrupoles is $d_1 = 15\,\mathrm{cm}$. The transformation matrix for this system is determined by multiplication transformation matrices of each optical element

$$\begin{pmatrix} x\,(z_1) \\ x'\,(z_1) \end{pmatrix} = \mathcal{M}_{QD}\mathcal{M}_{D_1}\mathcal{M}_{QF} \begin{pmatrix} x\,(z_0) \\ x'\,(z_0) \end{pmatrix}, \tag{3.1}$$

where the length of the full focusing system is $z_1 - z_0$, $\mathcal{M}_{QF}$ is a transformation

[1] The values used in this chapter were chosen as a typical specimen and for the study of an impact of individual elements of focusing system and fs beam tranpsort.

matrix of the focusing quadrupole (first focusing element)

$$\mathcal{M}_{QF} = \begin{pmatrix} 1 & l \\ -k_{\mathrm{f}} l & 1 \end{pmatrix}, \tag{3.2}$$

$\mathcal{M}_{QD}$ is a transformation matrix of the defocusing quadrupole

$$\mathcal{M}_{QD} = \begin{pmatrix} 1 & l \\ -k_{\mathrm{d}} l & 1 \end{pmatrix} \tag{3.3}$$

and $\mathcal{M}_{D_1}$ is a transformation matrix of the drift space between quadrupoles

$$\mathcal{M}_{D_1} = \begin{pmatrix} 1 & d_1 \\ 0 & 1 \end{pmatrix}. \tag{3.4}$$

Of course, if we want to know the position of the particle at $z_2 > z_1$, another drift space transformation matrix $\mathcal{M}_{D_2}$ has to be added with length $d_2 = z_2 - z_1$. Thus, the transformation is

$$\begin{pmatrix} x(z_2) \\ x'(z_2) \end{pmatrix} = \mathcal{M}_{D_2}\mathcal{M}_{QD}\mathcal{M}_{D_1}\mathcal{M}_{QF} \begin{pmatrix} x(z_0) \\ x'(z_0) \end{pmatrix}. \tag{3.5}$$

As could be seen from (3.2) and (3.3) matrices $\mathcal{M}_{QF}$ and $\mathcal{M}_{QD}$ can be written in the the same form which differs only by their focusing strength k_{f1} and k_{f2} given by (2.16). In this case, the focusing strength has to be negative for the defocusing quadrupole. Hence, in order to distinguish between focusing and defocusing quadrupoles, we will assign the positive magnetic field gradient g to the focusing quadrupole and negative to the defocusing quadrupole.

The trajectories of the particles in each energy line is shown in Fig. 3.1. Magnetic field gradients were chosen as $g_1 = 50\,\mathrm{T/m}$ and $g_2 = -50\,\mathrm{T/m}$ for focusing and defocusing quadrupole, respectively.

From Fig. 3.1 we can see, that the focal spot size is very large with a strog chromatic abberation. To correct this by sextupole, we firstly need to choose the position of the focal spot such, that particles with higher energies (above optical axis) will be focused and particles with lower energies will be defocused. To find the right position of the focal spot, we are interested only in two energy lines closest to the central energy line. The satisfying position is in the middle of the crossing of the optical axis by both energy lines (see Fig. 3.2). The chosen focal spot position is at $x = 1.825\,\mathrm{m}$.

The transformation matrix of the focusing system of the length $z_3 - z_0$ with added sextupole magnet is

$$\begin{pmatrix} x(z_3) \\ x'(z_3) \end{pmatrix} = \mathcal{M}_S\mathcal{M}_{D_2}\mathcal{M}_{QD}\mathcal{M}_{D_1}\mathcal{M}_{QF} \begin{pmatrix} x(z_0) \\ x'(z_0) \end{pmatrix}, \tag{3.6}$$

where $\mathcal{M}_S$ is the transformation matrix for the sextupole and has the same form as that for the quadrupole but the sextupole field gradient g_3 is positive above optical axis and negative below it.

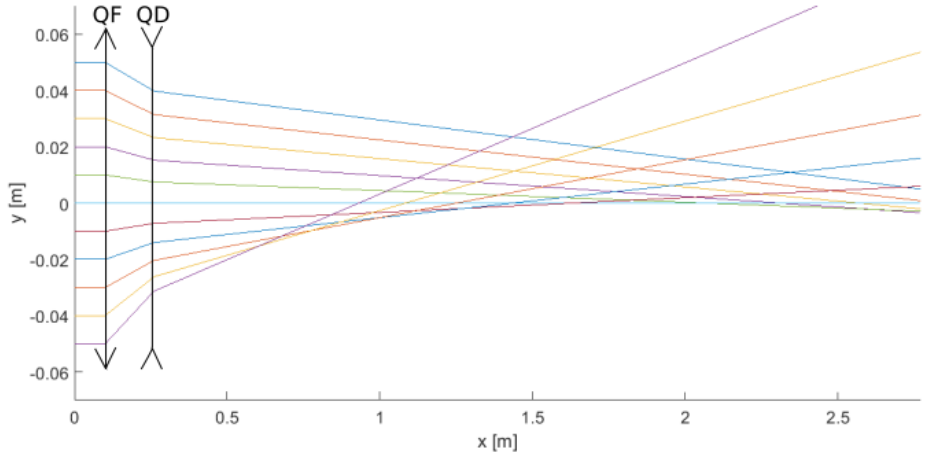

Figure 3.1: The electron beam propagation through focusing (**QF**) and defocusing (**QD**) quadrupoles. The energy of the particle in the top line is 110 MeV and the energy of the each line below that is decreased by 5 MeV.

The parameters are kept the same as that in the previous system and the drift length between the second quadrupole and the sextupole is also same $d_2 = d_1 = 15\,\text{cm}$. Finally, the position of the focal spot was chosen to $d_3 = z_4 - z_3 = 1.6\,\text{m}$. By adding another drift space $\mathcal{M}_{D_3}$ into the matrix system, the position x and slope x' of the particle at z_4 can be determined by

$$\begin{pmatrix} x\,(z_4) \\ x'\,(z_4) \end{pmatrix} = \mathcal{M}_{D_3}\mathcal{M}_S\mathcal{M}_{D_2}\mathcal{M}_{QD}\mathcal{M}_{D_1}\mathcal{M}_{QF} \begin{pmatrix} x\,(z_0) \\ x'\,(z_0) \end{pmatrix}, \tag{3.7}$$

Using (3.7) we can put the condition on the transversal position $x(z_4)$ of the particle, i.e. make the focal spot arbitrary small, and find the optimal field gradient of the sextupole g_3 iteratively.

The particle trajectories propagating through this focusing system are shown in Fig 3.3, where we choose the condition $x(z_4) < 0.05\,\text{mm}$. Therefore, the focal spot size diameter is less than 0.1 mm. The corresponding sextupole field gradients g_3 for each energy line are shown in Fig. 3.4. For energy lines above the mean value, the field gradient is positive and negative below the axis, which is desired. The absolute value of the field gradient is growing with the increasing distance from the beam axis.

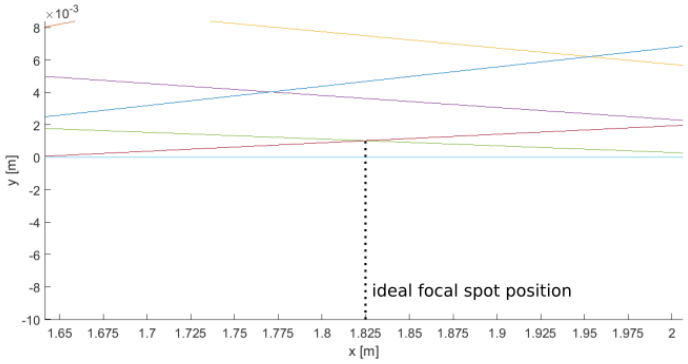

Figure 3.2: Zoomed Fig. 3.1. Finding the ideal focal spot position.

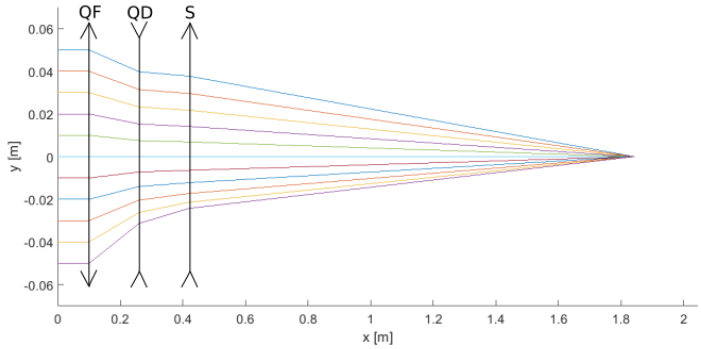

Figure 3.3: The electron beam propagation through focusing (**QF**) and defocusing (**QD**) quadrupoles and sextupole (**S**). The energy of the particle in the top line is 110 MeV and the energy of the each line below that is decreased by 5 MeV.

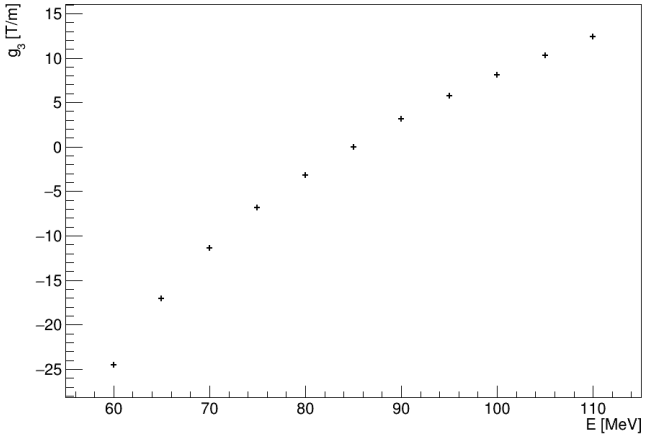

Figure 3.4: Dependence of the sextupole magnetic field gradient g_3 (in the quadrupole approx.) on the energy line E.

Chapter 4

Electron beam spatial chirp

An important part of our focusing system is a device providing electron beam spatial chirp. Without this part the proper sextupole correction would not be possible (see Sec. 2.4).

4.1 Design

To spatialy chirp the electron beam, the set of two dipole magnets can be used. The considered scheme is shown in Fig. 4.1. Since the radius of the electron trajectory in the magnetic field grows with a higher velocity by (2.7), the electrons with the higher energy are deflected less then those with the smaller energy. Thus, the first dipole magnet separates the beam by energies, which increases the beam size. The importance of the second dipole magnet is mainly to collimate the beam and to get the propagation direction back to the initial one.

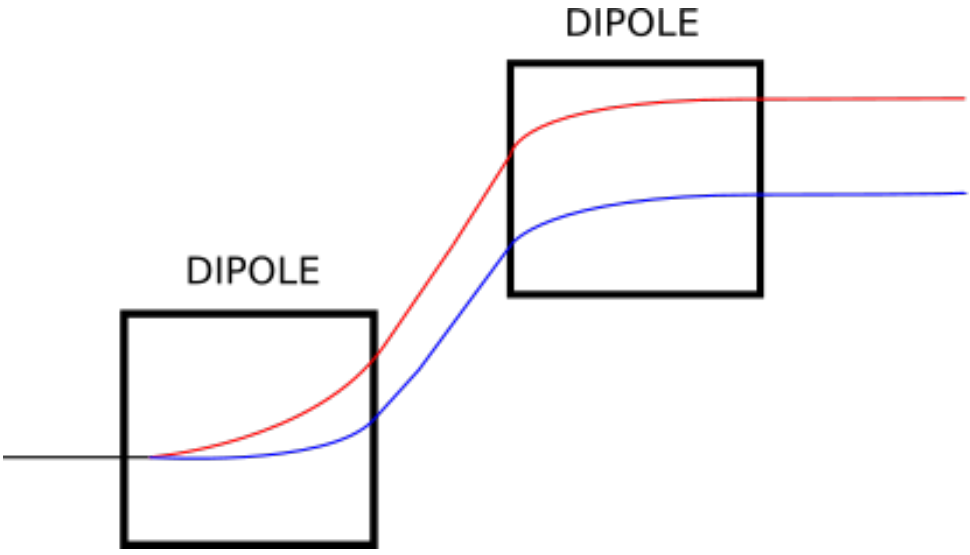

Figure 4.1: The scheme of spatial chirp of the electron beam by two dipole magnets. Higher energy particle (blue) trajectory is bended less than lower energy particle (red) trajectory.

To get an energy chirped electron beam, which is collimated, the magnitude of the magnetic field of both dipole magnets has to be the same (with the opposite orientation of the magnetic field). Moreover, the length of both magnets in the direction of the beam propagation has to be also identical.

The size of the chirped beam depends on many aspects. The most important values are the initial paramteres of the beam, such as initial energy, energy spread and a beam divergence. The beam size also depends on the distance between the dipole magnets and the magnitude of their magnetic fields. A comparision is shown in Sec. 4.2.

4.2 Simulation

The simulation of the energy chirp of the electron beam is performed using SIMION software. Two dipole magnets are used. Their length is set to 17.5 cm and magnetic field to 0.2 T. The energy of the initial beam is fixed and uniformly distributed with energies from 20 MeV to 40 MeV.

Suppose, the chirped electron beam with diameter of 10 cm is needed. The diameter of the initial beam is set to 1 cm and the beam has no divergence. The only free parameter, which could change the diamater of the chirped beam is the distance between dipole magnets.

For parameters mentioned above, the correct distance between dipoles to obtain a 10 cm diameter beam is determined as 13.5 cm. The beam chirp can be seen in Fig. 4.2. The distribution of the position of particles in y axis perpendicular to the beam propagation direction is shown in Fig. 4.3.

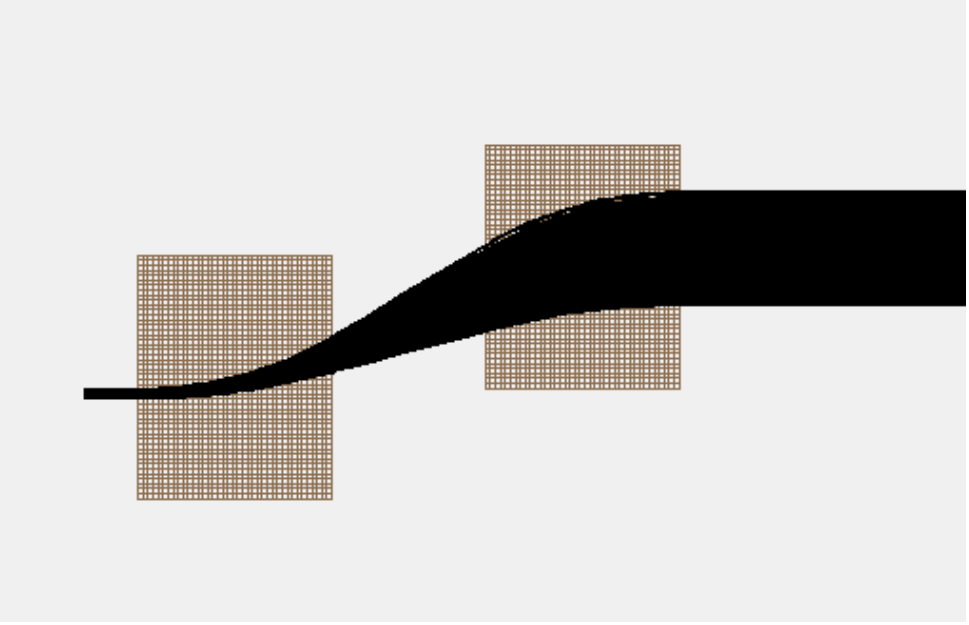

Figure 4.2: The spatial chirp of the electron beam with energies from 20 MeV to 40 MeV, radius 5 mm and zero divergence.

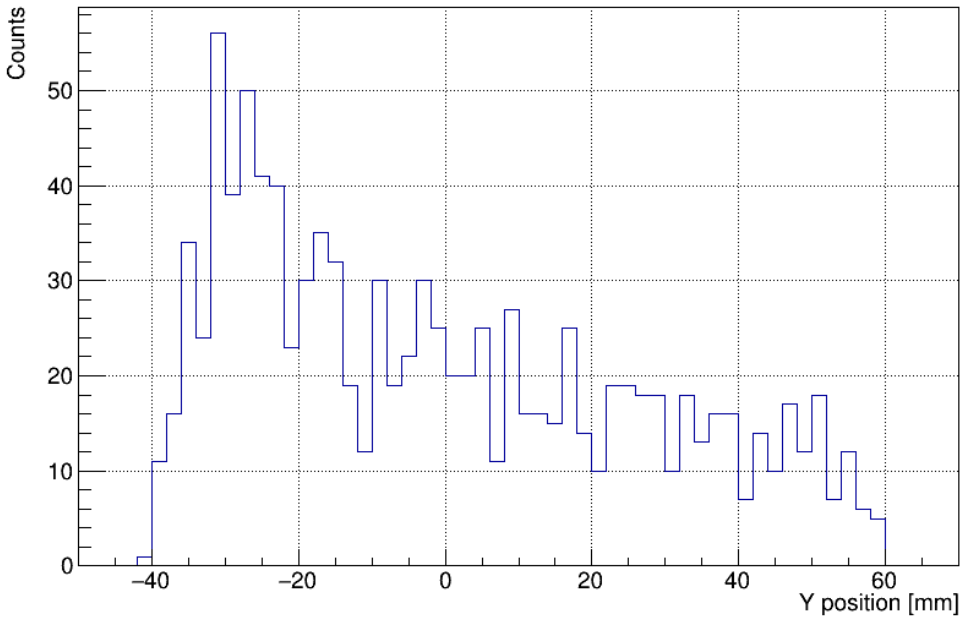

Figure 4.3: Distribtion of the electron transverse position in the beam with 10 cm diameter.

From Fig. 4.3, it can be seen that particles located below $y = 0$ value are closer to each other, even though the beam energy is distributed uniformly. The mean value $y = 0$ corresponds to the central beam energy (30 MeV). This is expected due to the relation (2.7). The beam trajectory is curved twice, thus higher energy particles are curved by a small radius also twice and the final y position change is much smaller than that of the slower particles.

As mentioned earlier, the size of the chirped beam can be changed by adjusting the distance between dipole magnets. However, the relation is not simple and the chirped size cannot be computed easily since there is also a strong dependence on a dipole magnetic field, its length and beam energy.

For comparision, we found the position of the second dipole magnet to obtain a chirped beam with approximately 15 cm in diameter. The distribution of a transverse position of electrons is in Fig. 4.4. The distance between the dipole magnets was determined to 28 cm.

The relation between the final beam size and the dipole position could be found if more simulations would have been provided. Nevertheless, the beam size does not have any impact on the focusation by the quadrupoles.

Although, the focal length of the sextupole magnet is dependent on a distance from its axis. The beam size at the entrance of the sextupole can be changed by both quadrupole magnetic field strength and the distance between the second quadrupole and the sextupole.

The size of the chirped beam is affected by the initial size much less than

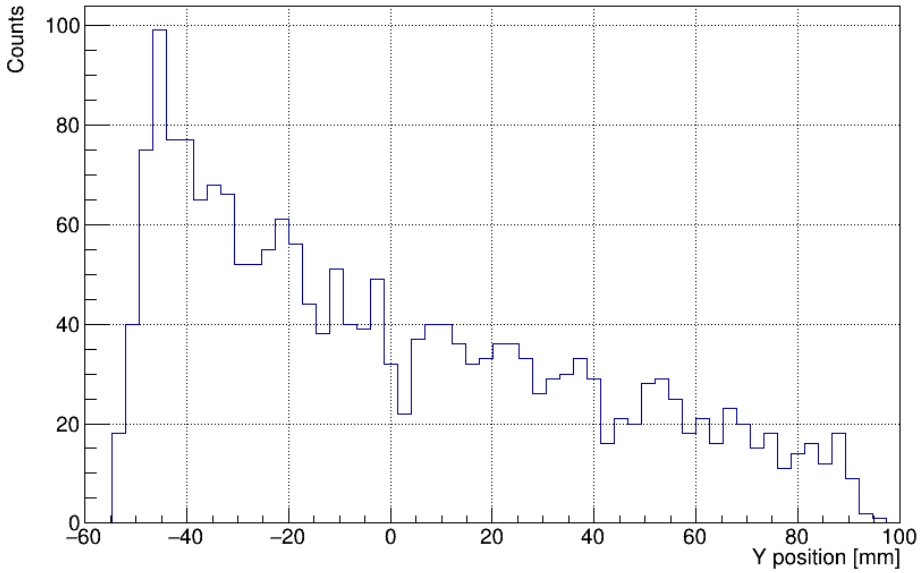

Figure 4.4: Distribtion of the electron transverse position in the beam with 15 cm diameter.

by other parameters mentioned earlier. The difference is absolute because only the inital position of each electron is changed. More crucial parameter, that changes the chirped beam, is the initial beam divergence.

The spatial chirp of the beam with a half divergence of one degree is shown in Fig. 4.5. As it could be seen the chirped beam is also divergent. The divergence of the chirped beam was estimated by measuring its size in two different positions to approx. 0.86 degree. Hence, the final divergence is slightly reduced compared to the initial one.

To colimate this beam, a sector magnet might be used instead of the second dipole, by which particles with lower energy would spent more time in the second magnet, hence their trajectories would be more curved. Whereas, the distance in the second magnet would be smaller for higher energy particles, which would also straighten their trajectories.

Fortunately, electron beams, which are accelerated by laser wakefield acceleration, usually have divergences even smaller (around 10 mrad). Therefore, the chirped beam has a small divergence and a correction by sector magnet is not needed.

4.3 Scaling for different beam energy

Since electron beams with different energies can be produced by LWFA depending on different injection mechanisms and other laser-plasma conditions, the scaling for energies has to be provided.

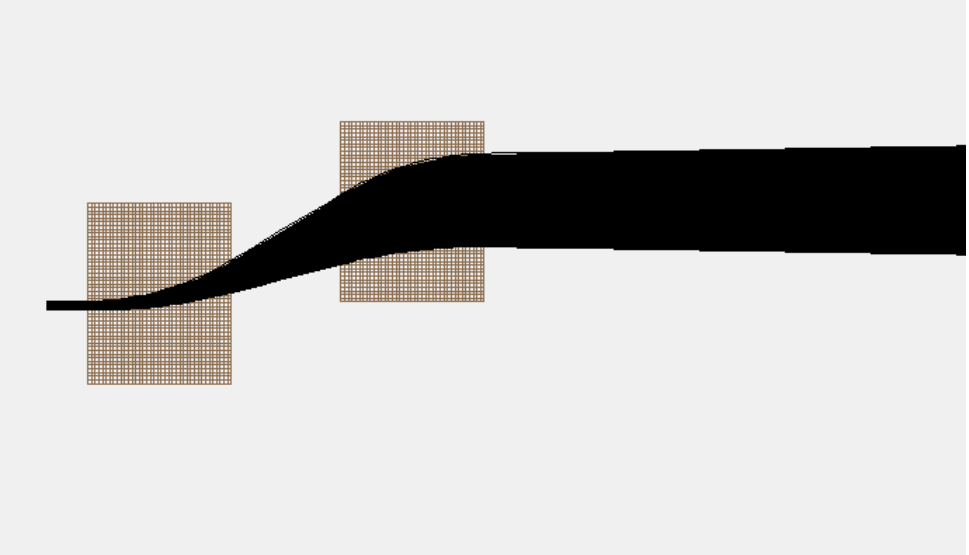

Figure 4.5: Chirp of the beam with a half divergence 1 degree.

If there was no change in set of parameters described above, the beam would be still colimated and chirped. However, the beam size would be changed, which might lead to increasing the size of the focal system. Moreover, the central position would be more shifted so it would be challenging to find the correct optical axis.

The simplest way to provide scaling is to adjust the magnetic fields of the dipole magnets. The goal is to produce the same beam size for different energies. Using formula (2.7) the curvature radius of the particle trajectory can be calculated. To obtain the same beam diameter, the difference in the curvature radius of the particle trajectory with the highest energy and that one with the lowest energy has to be identical to that mentioned in the previous section. If this is guaranteed the slowest electron will enter the drift space between magnets in the same position and with the same slope as the slowest electron in the case performed in the previous section. This is also valid for the fastest electron.

The difference between curvature radii ρ_1 for $E_1 = 20$ MeV and ρ_2 for $E_2 = 40$ MeV electrons in a magnetic field of 0.2 T can be calculated by

$$\rho_2 - \rho_1 = \frac{\beta_2 E_2'(\mathrm{GeV}) - \beta_1 E_1'(\mathrm{GeV})}{0.2998 B(\mathrm{T})} \doteq 33.36 \text{ cm}. \tag{4.1}$$

Hence, the magnetic field required to obtain 10 cm diameter beam for the beam with energies from E_1' to E_2' is

$$B(\mathrm{T}) = \frac{\beta_2 E_2'(\mathrm{GeV}) - \beta_1 E_1'(\mathrm{GeV})}{0.2998 \cdot 0.3336}. \tag{4.2}$$

The particle velocity fraction $\beta = \frac{v}{c}$ can be set to 1 for highly relativistic partices. However, for less energy electron it can be determined using the

basic relativistic formula for energy

$$E_{kin} = E_0(\gamma - 1), \tag{4.3}$$

where E_{kin} is the kinetic energy of the particle, E_0 its rest energy and $\gamma = \frac{1}{\sqrt{1-\beta^2}}$ is the Lorentz factor. Thus,

$$\beta = \sqrt{1 - \left(\frac{E_0}{E_{kin} + E_0}\right)^2}. \tag{4.4}$$

Of course, very high relativistic beams will require much higher magnetic fields than those, which are affordable. In this case, it would easier to elongate the dipole magnet.

Chapter 5

Focusing system

Since the beam accelerated in an accelerator evolves when propagating in space, the focusing system is needed for the beam transport to keep the size of the beam small, which means focusing particles with different energies into one spot. The focusing systems in conventional accelerators are achromatic but usually works with a minimal energy spread. The focusing system we propose focuses electron beams with larger energy spread in both perpendicular and longitudinal direction.

5.1 Focusing system design

Our focusing system consists from all parts, that are mentioned in previous two chapters. Namely two dipole magnets for a beam chirp, two quadrupole magnets for focusing and the sextupole magnet for the achromatic correction. The scheme of this system is shown in Fig. 5.1.

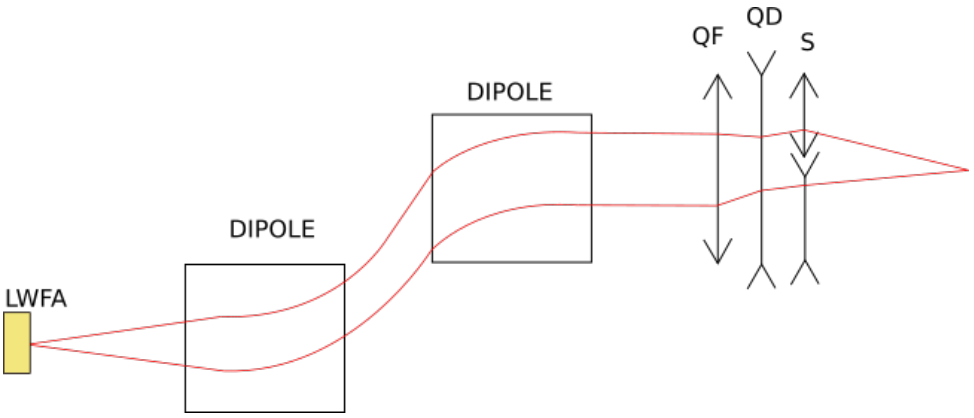

Figure 5.1: Scheme of a focusing system.

As one can see from a scheme, the beam focusing is mainly provided only in one plane. In the other plane, the electron beam is not chirped. Hence, the beam size remains the same as the initial one. Considering that the initial beam is very small and it is propagating along optical axis of both quadrupoles, where the magnetic field is compensated from all poles of quadrupole, there

would be no force to curve particle trajectories and the beam size would no be changed. Similarly, the force acting on a particle close to the centre of the sextupole would be very small. Therefore, the beam size is not changed in the other, where the beam is not chirped.

5.2 Positioning quadrupole magnets

Although the beam is mainly focused in one plane, finding the same focal length in both planes is desirable. Therefore, the correct distance between the quadrupole magnets must be estimated. When the ideal focal length is found for a central energy of a beam (propagating in optical axis, when the beam is chirped), it guarantees, that higher energy electrons will be focused further and lower energy electrons closer.

Finding the correct distance between the quadrupoles was provided in Matlab. Considering the beam with the same parameteres as in Chap. 4. The central beam energy is then 30 MeV. The distance was determined iteratively. The process was similar to that in Chap. 3 with a difference that a thin lens approximation was not used because the quadrupole length was set to 6 cm. If the quadrupoles are closer to each other, the focal length in a plane, where the first quadrupole is focusing and the second one is defocusing, is increasing and vice versa. From the simulation it was found out, that the field strength of the quadrupoles has to be different. If not the focal length is very long.

Of course, magnetic field strength of each quadrupole can be chosen arbitrary, which would change both the distance between the quadrupoles and the focal spot position (Choosing the ideal magnetic field strength is in Sec. 5.4). The magnetic field gradient of the first quadrupole is set to 4 T/m and of the second quadrupole is 5 T/m.

Using these parameters the distance between quadrupoles was determined as 137 mm. The focal spot was distanced 767 mm from the end of the second quadrupole. Focusing of 30 MeV in both planes is shown in Fig.5.2.

5.3 Simulation in SIMION

Next simulation is performed again in SIMION. The quadrupoles are created with both width and heigth 30 cm and thickness 6 cm. The distance between the tip of magnetic poles, which are in the opposite side of the magnet is 7.5 cm. Their magnetic fields are set in such a way, that they correspond to field strengths used in Matlab simulation, i.e. 4 T/m and 5 T/m for the first and the second quadrupoles, respectively. The sextupole height and width are 20 cm with distance bewteen opposite poles of 2.5 cm. Its thickness is 6 cm.

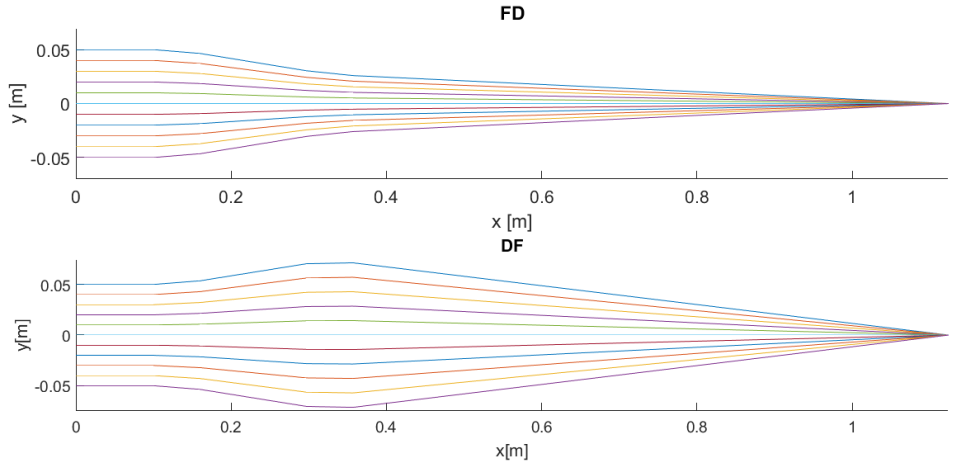

Figure 5.2: System of two quadrupoles with the same focal length in both planes.

5.3.1 Monochromatic beam focusing

Firstly, monochromatic beam with 30 MeV energy is focused by two quadrupoles. The inital beam diameter is 4 cm and has no divergence. The focal spot size in both planes is around 20 µm and it is located approximately 768 mm from the second sextupole, which is in coincidence with Matlab simulation. Focusing in both planes is shown in Fig. 5.3.

5.3.2 Focusing of electron beam with energy from 25 MeV to 35 MeV

In this part, we combined dipole magnets, the quadrupole magnets and sextupole to create a system shown in scheme Fig. 5.1. The parameters, such as magnet dimensions and their magnetic fields are taken identical to those used in previous sections.

The initial beam diameter is set to 2 mm and its energy is uniformly distributed from 25 MeV to 35 MeV. The reason of not using energies from 20 MeV to 40 MeV (which were used earlier) comes from a Matlab simulation. We tried to find the magnetic fields which would correct chromaticity similarly to those performed in Chap. 3 with an exception of not using thin lens approximation and treating the sextupole as a quadrupole (focusing and defocusing in each half-plane). However, trajectories of electrons with energies below 25 MeV are crossing each other even before entering the sextupole. Thus the lowest energy trajectory would require higher magnetic field while it is located closer to the centre of the sextupole than the electron with the higher energy, which is situated further. This could be corrected either by placingthea sextupole closer to the second quadrupole or by adjusting the magnetic field of the quadrupoles. The energy cut off is provided only for simplicity.

The distance between the sextupole and the second quadrupole is fixed

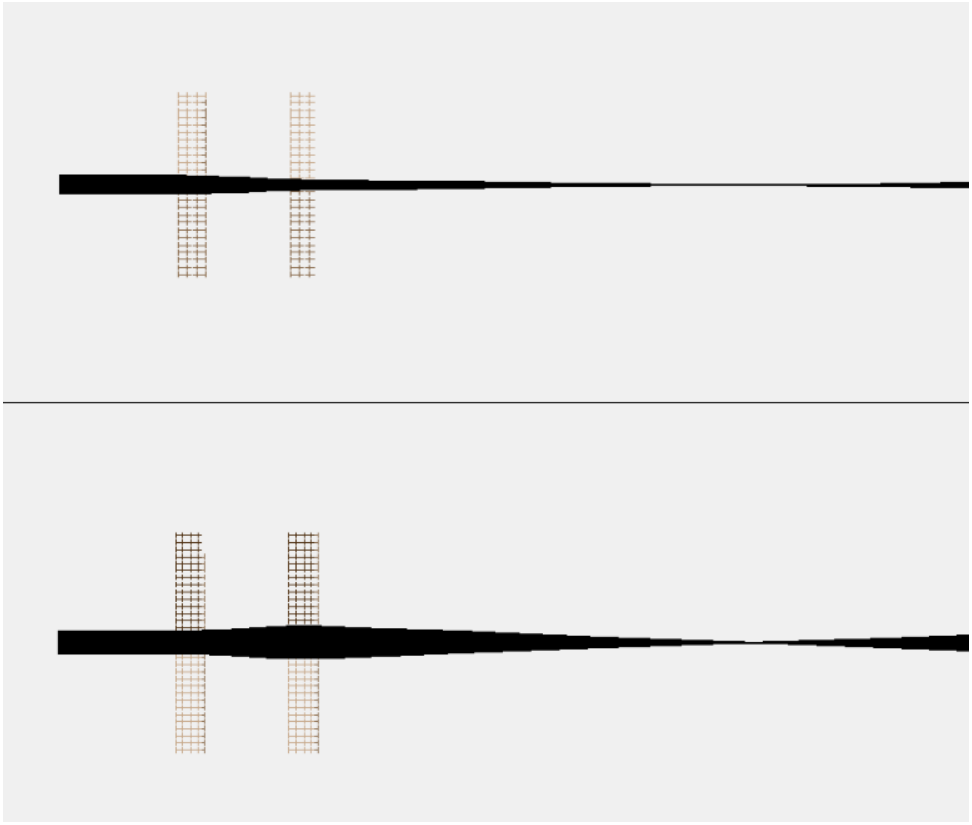

Figure 5.3: Focusing of 30 MeV electron beam (black) by two quadrupoles (brown rectangles) in both planes in SIMION.

to 5 cm. Thus, the only free parameter left to correct beam chromacity is sextupole magnetic field strength. The method of finding the proper value is based on using 3 monoenergetic electron beams with energies: 35 MeV, 25 MeV and 30 MeV, which defines the optical axis. Each beam is 0.02 mm in diameter and all of them start at the same point.

The sextupole magnetic field is being adjusted until all trajectories are crossing each other at the same spot. The final achromatic correction is shown in Fig. 5.4, where blue trajectory corresponds to an energy of 35 MeV, black to 30 MeV and red to 25 MeV. The sextupole field gradient was determined to 1.41 T/m (in the quadrupole approximation).

The position of the focal spot is approximately 460 mm from the edge of the second quadrupole, which is much closer than the focal length of the monoenergetic 30 MeV beam focused by the quadrupoles with the same parameters. The size of the focal spot is shown in Fig. 5.6 and Fig. 5.7. The asymmetry in beam profile in y-axis is again due to nonlinear spatial chirp, in z-axis the beam remains very small and propagates through the centre of magnets where the field is very weak and only electrons near the beam periphery are affected by it. Finally, the 3D model of the achromatic focusing system, where 25-30 MeV electron beam is blue and 30-35 MeV beam is red,

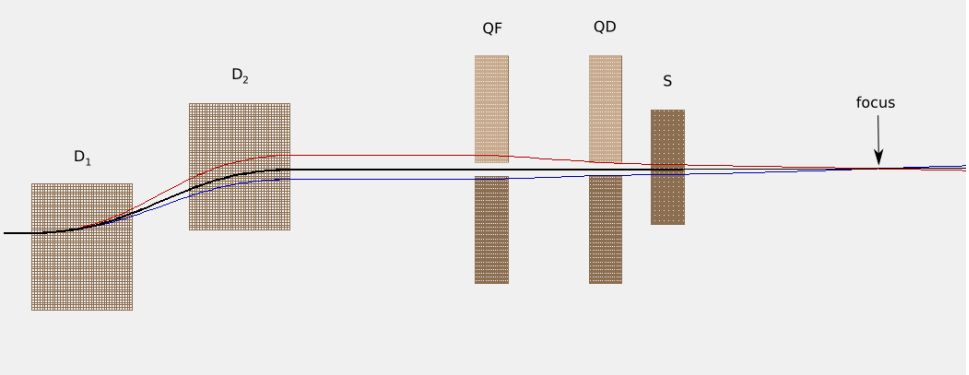

Figure 5.4: Finding the same focal spot of electron beams with energies: 35 MeV (blue), 30 MeV (black) and 25 MeV (red) by focusing system consisted of the dipoles $\mathbf{D}_1$ and $\mathbf{D}_2$, the focusing quadrupole **QF**, the defocusing quadrupole **QD** and the sextupole **S**.

is shown in Fig. 5.5.

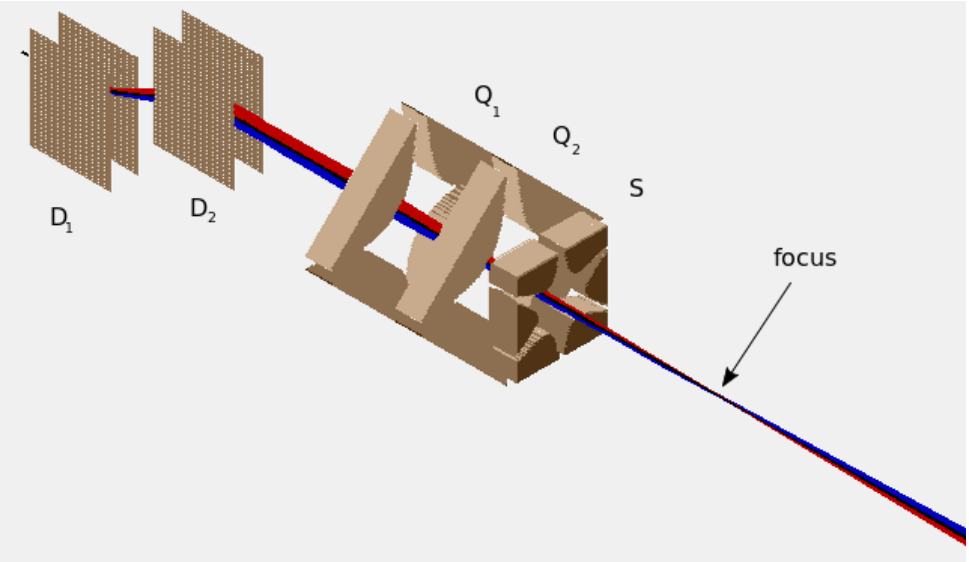

Figure 5.5: 3D model of achromatic focusing system: the dipoles $\mathbf{D}_1$ and $\mathbf{D}_2$, the focusing quadrupole **QF**, the defocusing quadrupole **QD** and the sextupole **S**. Electrons with energy 25-30 MeV (red) and 30-35 MeV (blue).

5.3.3 Time of flight

In Fig. 5.8 time of flight (TOF) electron distribution is shown to see the longitudinal size of the beam in the focal spot. The decreasing tendency is also due to the nonlinear spatial chirp. The distance which electrons travelled in a propagation axis x from start to focal spot is 1530 mm. It can be seen

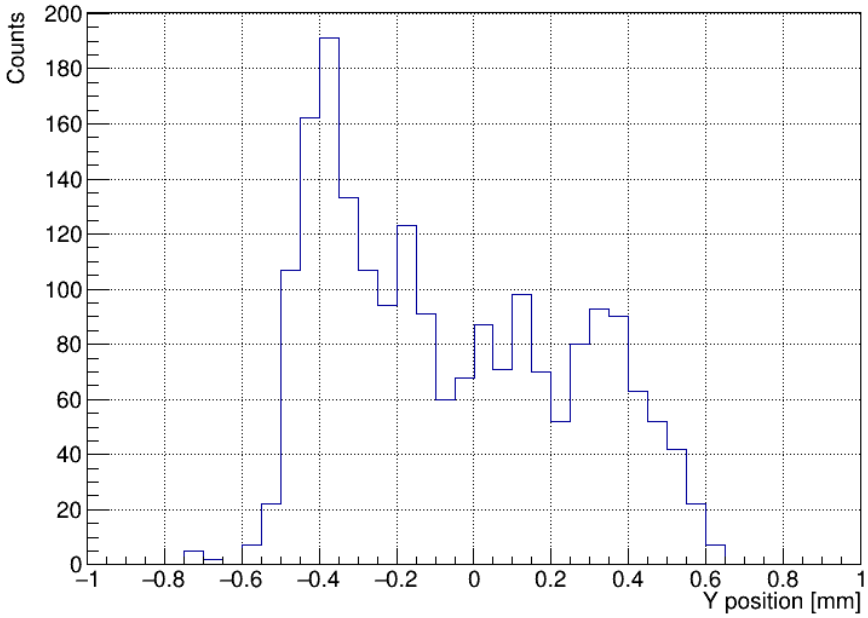

Figure 5.6: Distribution of electron positions in the focal spot in y-axis.

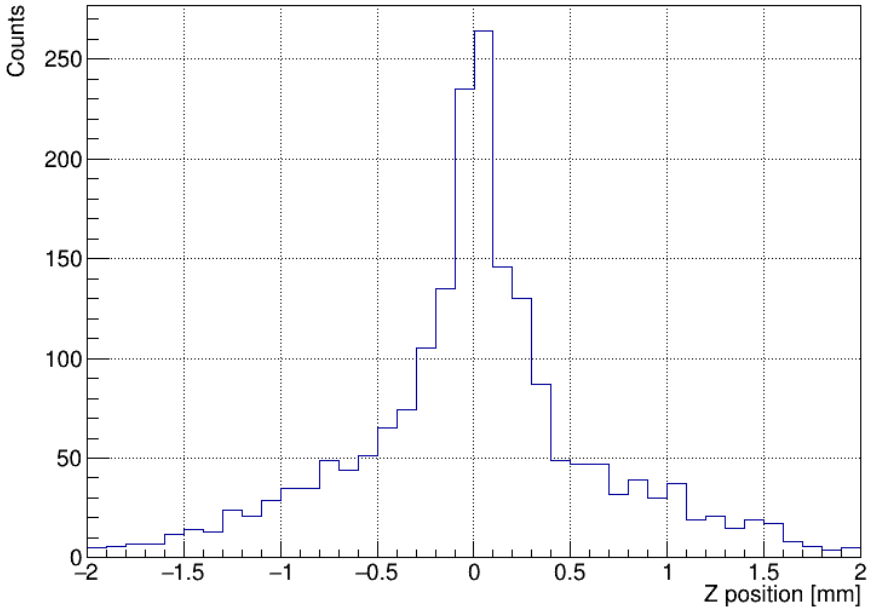

Figure 5.7: Distribution of electron positions in the focal spot in z-axis.

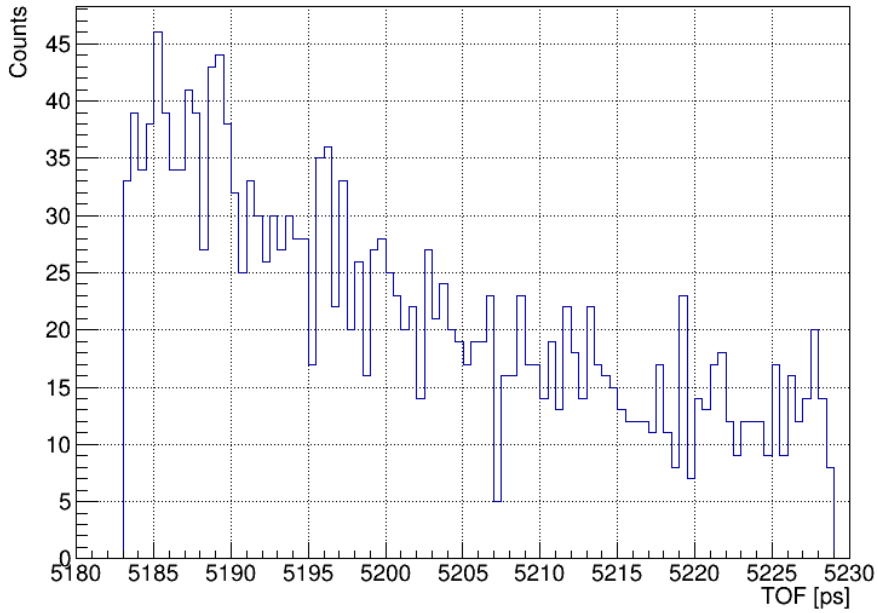

Figure 5.8: Time of flight distribution of electrons (in the focal spot) travelling distance of 1531 mm.

that the beam elongated to 46 ps, which corresponds to 14 mm for relativistic particles ($v \simeq c$). An isochronous correction for this focal system is proposed in a next section.

5.4 Isochronous correction

Another step is a dealing with the longitudinal focusation. In Fig. 5.9 the dependence of TOF on the electron energy is shown, where it can be seen, that more energetic electrons come into the focal spot sooner than less energetic electrons. Hence, it has to be ensured that the higher energy electrons enter the focusing system with a certain time delay. In other words the trajectory of faster electrons has to be extended and vice versa.

In this case the magnetic chicane, which is mainly used as a beam compressor in conventional accelerators, would not work because it provides exactly the opposite, i.e. elongates the trajectory of the slower particles.

One of the possible approaches (another method is described in Chap. 6) to compensate the slower particles time delay is directing the lowest energy line to the centre of the focusing system. Then, the trajectories of the slowest particles would not be changed and other electron path lengths (distance between first quadrupole and focal spot) would be proportional to their energy.

However, the focusing system, which is described in previous sections, has

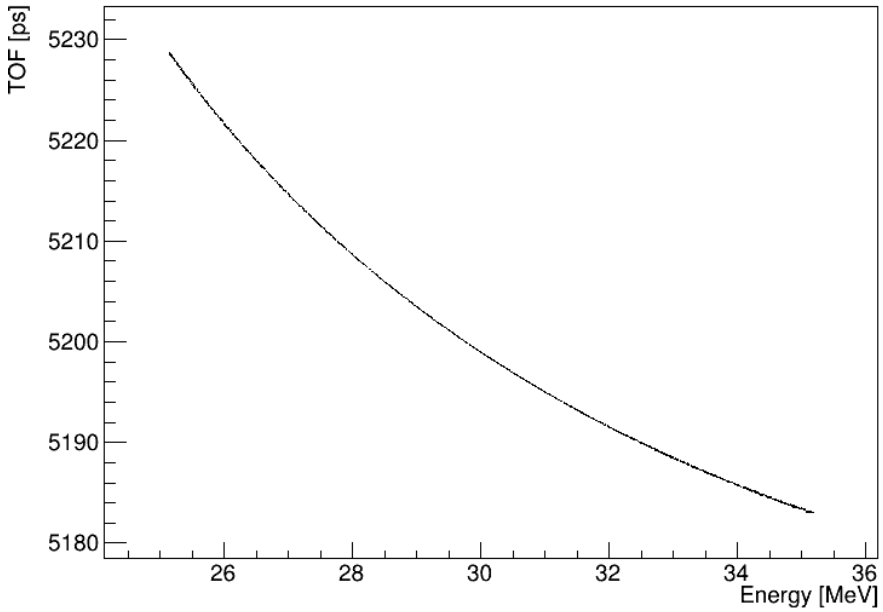

Figure 5.9: The TOF dependence on electron energy at focal spot distant 1531 mm from the beam creation.

to be slightly modified. Although it is possible to use the same system, the delay would not be sufficient since the difference in TOF is very large. This could be improved if the focal length of whole focusing system is decreased, which can be provided by adjusting the quadrupole and sextupole magnetic fields. Nevertheless, it is rather complicated to find the ideal fields magnitude.

Another improvment might be by increasing a diameter of the chirped beam. This would also increase the distance, which faster particles must travel to focal spot but simultaneously it would make bigger difference in TOF of particles before they enter the first quadrupole because slower particles would have to travel even longer path between the dipole magnets.

The easiest modification of the focusing system, that broadens the beam, is switching the quadrupole magnets, such that the first quadrupole is defocusing (in a plane, where the beam is chirped) and the second quadrupole is focusing. Then, if the distance between is increased, the more energetic particles become more distant from the centre. Advantage is that the beam is firstly focused in other plane (note that the beam is small before entering the first quadrupole) and approaches the optical axis, which means that the size is not changed much by neither the second quadrupole nor sextupole field. Thus, finding the same focal length in both planes is not necessary. Moreover, the sextupole correction is only in one half-plane. The only limiting parameter is the focal length of the first quadrupole, which must not be shorter than distance between quadrupoles and also the second quadrupole has to be large enough

to accept the whole beam.

Of course, when this modification is applied, a new proper value of the sextupole magnetic field must be found to correct the chromacity. The simplest method which may be used optimize the beam TOF is to ensure (by increasing the distance between the quadrupoles), that the fastest particle crosses the focal spot as the last one. Knowing the time of arrival in the focal spot for the first particle (slowest) and the last (fastest), we can calculate a proper additional drift space length between the dipole and the quadrupole for the correction.

Using (2.15) and (2.16) the focal length of the first quadrupole is $f_{Q1} = 347\,\text{mm}$, where energy of 20 MeV was used to find a lower estimate. Hence, the second quadrupole and sextupole placed 200 mm from previous position in other to not crossing focal length. Graph of TOF dependence on the electron energy in the focal spot is shown in Fig. 5.10. However, now it can be seen, that this correction works only for higher energies but might not be possible for lower (or mid range) energy electrons. The reason is following. When the beam is chirped, trajectories of the slowest electrons are elongated too much that this correction is not sufficient.

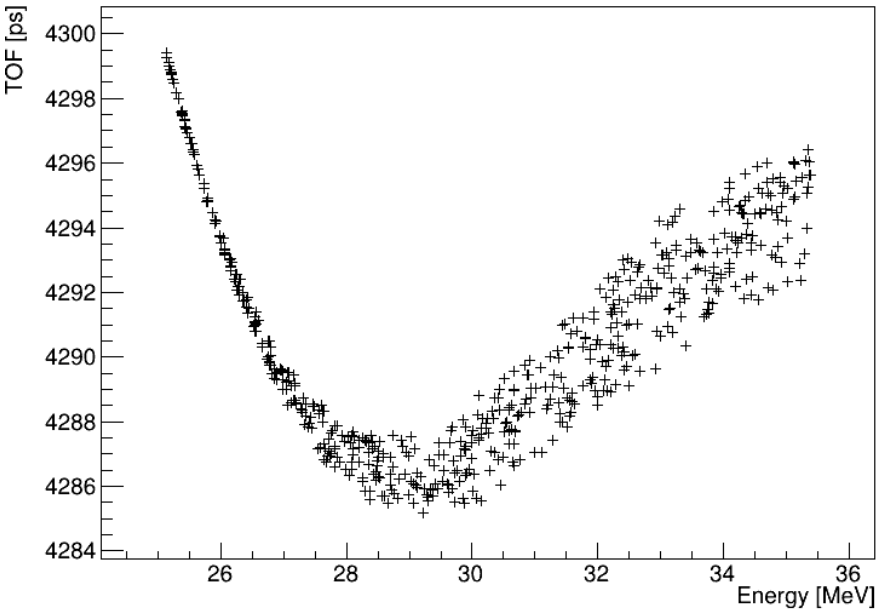

Figure 5.10: The TOF dependence on electron energy, when the beam is more expanded by quadrupoles.

Even if the radius of the chirped beam is reduced and the difference between the trajectory lengths is smaller, another issue comes out. Particle trajectories of lowest energy levels are very close to the centre of the magnet, which means that tremendous magnetic field gradients has to be applied to compensate them. On the other hand, the particles further from the centre are kicked so

far, that they arrive to the focal spot region much later, hence they cannot be compensate by extending a drift space. Moreover, the quadrupoles with huge magnetic strengths have a very short focal length, therefore in the second plane a very divergent beam would be created. Therefore, other method for time correction has to be applied.

Chapter 6

Isochronous correction by reversing the beam

As shown in previous chapter an isochronous correction only by positioning the beam (or magnets), in order to send the slowest particles to the centre of the focusing, is not sufficient. This compression uses only focusing system (quadrupoles and sextupole). Therefore, the beam has to be shaped even before it reaches the first quadrupole.

The aim is still to get less energy electrons ahead of faster ones. For this purpose, we propose reversing the beam in the opposite direction. By (2.4) the faster electrons would need larger radius to be directed back. Furthermore, the beam would be also spatially chirped.

6.1 Reversing the electron beam

Reversing the electron beam can be provided simply by the dipole magnet. The schematic picture of the reversed beam is shown in Fig. 6.1.

Reversing leads to an advantage, such that the size of the chirped beam can be determined precisely since there is only one magnetic field. Using (2.4) the size of the beam is

$$D = 2(\rho_1 - \rho_2) = 2\frac{\sqrt{E_1^2 - E_{1,0}^2} - \sqrt{E_2^2 - E_{2,0}^2}}{Bce}, \tag{6.1}$$

where E_1 and $E_{1,0}$ is the total energy and the rest energy of the most energetic particle, respectively and E_2 and $E_{2,0}$ is the total energy and the rest energy of the least energetic particle, repsectively.

Morevover, TOF difference Δt between electrons, when exiting the magnet can be calculated from

$$\beta_{1,2} = \frac{v_{1,2}}{c} = \frac{l_{1,2}}{t_{1,2}c}, \tag{6.2}$$

where $l_{1,2} = \pi\rho_{1,2}$ is the trajectory length of the fastest and the slowest electron in a dipole magnet, respectively. Hence, the time difference is

$$\Delta t = t_1 - t_2 = \frac{\pi}{c}\left(\frac{\rho_1}{\beta_1} - \frac{\rho_2}{\beta_2}\right). \tag{6.3}$$

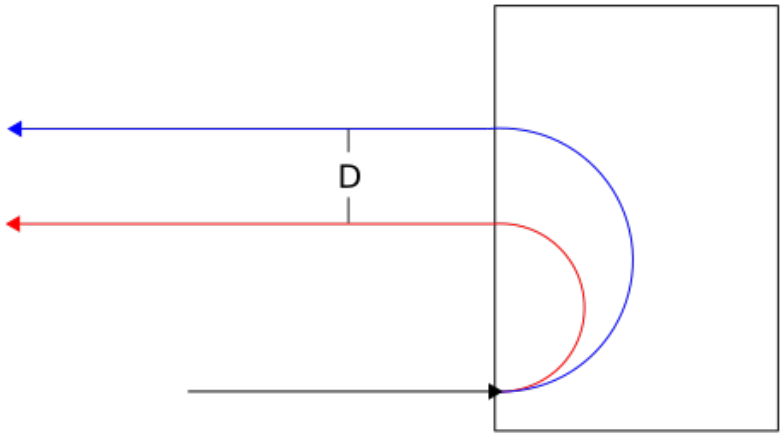

Figure 6.1: Reversing the electron beam by dipole magnet. The low energy electrons (red) are curved more than the high energy electrons (blue).

When particles are ultra-relativistic, relations (6.1) and (6.3) become linearly dependent on energy, because $E \gg E_0$ and $\beta \simeq c$ in ultra-relatvistic limit. Consequently, the distribution of a transverse position of the electron in the beam and TOF dependence is also linear in the energy. This is a vital property, when compared to chirping by two dipole magnets. From Fig. 5.10 it would be necessary to slow down the electrons possessing middle range energy, which leads to very challenging task. Whereas, using the reversed beam the compression can be achieved more easily. The issue arises in finding the suitable compressor, which compresses also linearly in the energy.

Due to a spatial beam distribution, in which fast particles are located in the rear end, the elongation of the drift space might be used. Consider again the electron beam with energy 20-40 MeV and a dipole magnet with magnetic field of 1 T. The radii for the fastest and the slowest particles are $\rho_1 = 135.12\,\text{mm}$ and $\rho_2 = 68.39\,\text{mm}$, respectively. Notice, that for these energies the expression for the curvature radius is still not linear enough ($\rho_1 \neq 2\rho_2$). The time difference between them is $\Delta t \doteq 699\,\text{ps}$.

A simple calculation can be provided to estime how long the drift space must be, such that the 40 MeV electrons catch up 20 MeV electrons. Let s be the required drift length. The expression for s is found using (6.2) and $t_2 = t_1 + \Delta t$ as

$$s = \frac{\beta_2 c \Delta t}{1 - \frac{\beta_2}{\beta_1}}. \tag{6.4}$$

The required drift length for this beam is approximately 9 km. Thus, the compression only by propagation in the space is not possible.

For less energetic beams ($\approx$ MeV) the calculated drift length is in the order of metres. However, for these energies the compression by drift space is not linear and TOF dependency on energy reaches similar distribution as that in Fig. 5.10.

6.2 Sector magnetic chicane compression

The result of the previous section indicates, that a compression system must be employed into our focusing system, since the drift space needed for longitudinal focusation is far too long.

The compression system widely used in conventional accelerators is a magnetic chicane. This system consists of four dipole magnets. The basic idea is to spatialy chirp the beam and collimate it (as shown in Chap. 4) and then using a mirrored geometry to compress the beam back to initial size. Hence, less energy particles travel longer distance than more energetic ones, which leads to compression.

However, for our purpose this simple magnetic chicane cannot be used as it stands, because same nonlinearities would arise leading to U-profile TOF distribution again. Hence, an improvement which preserves linear TOF distribution has to be applied.

6.2.1 Sector magnet

To achive the desired modification we suggest to replace the simple rectangular dipole magnets by the sector magnets. The sector magnets are similar to the dipoles but with edges cut by a certain angle. They possesss a suitable property, such that if the configuration is properly set, the sector magnets deflect the collimated beam by an angle without any change of its size (if the beam is firstly chirped before the entrance).

Propagation of the beam through the sector magnet is shown in Fig. 6.2. As can be seen, the beam enters the magnet at 90 degree angle with respect to the magnet edge and exits also at 90 degree angle. The important part is to place the magnet correctly into to the beam trajectory and use the right magnetic field, so the beam is deflected by the same angle as between magnet edges.

In our case (considering a hard edge model) the beam size is $D = 2\,(\rho_1 - \rho_2)$. From Fig. 6.2 it follows that new curvature radii satisfy

$$r_1 - r_2 = 2\,(\rho_1 - \rho_2)\,, \tag{6.5}$$

thus $r_{1,2} = 2\rho_{1,2}$, which implies that the magnetic field of the sector magnet must be a half of the strength of the dipole field used for the beam reversion. Consequently, the lowest energy line of the beam must enter the magnet exactly at the distance r_2 from the sector centre.

The angle of deflection of the beam corresponds to the sector angle α, which can be chosen arbitrary. It follows that the beam direction can be changed by the geometry of the sector magnet (its angle) and not by changing the magnitude of a magnetic field, because if the magnetic field is changed the beam leaving the magnet is divergent.

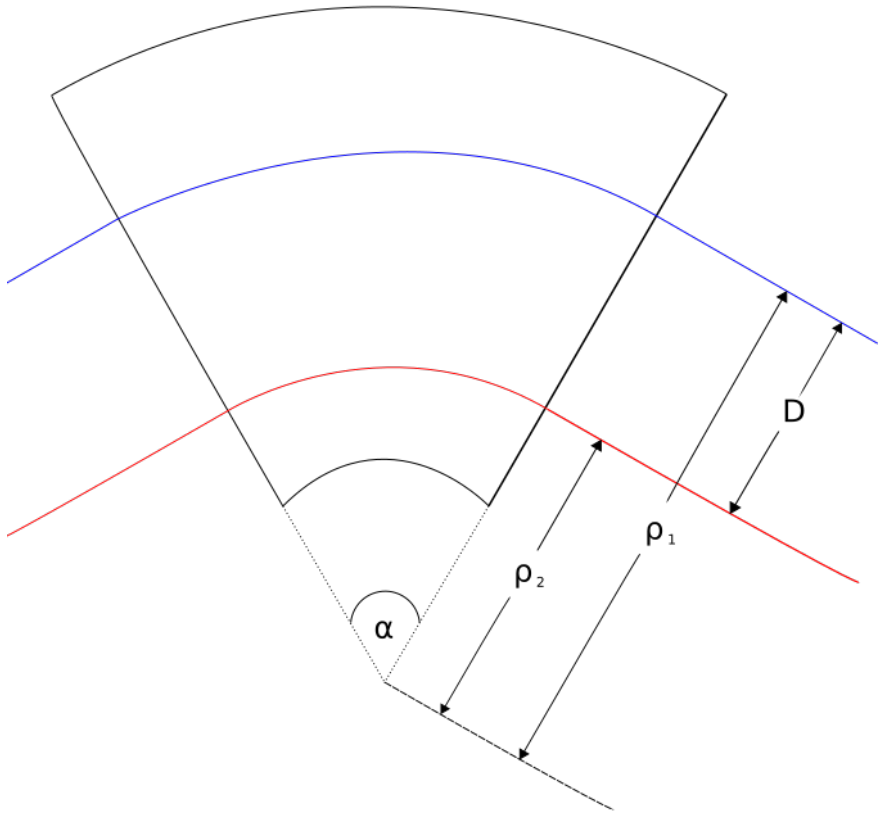

Figure 6.2: The beam propagation through the sector magnet. The high energy elecrons are curved by radius ρ_1 the low energy electrons (red) are curved by radius ρ_2 . The beam is deflected by the sector angle α.

6.2.2 Chicane design

However, at this point (after the deflection by the sector magnet) the beam only changes its propagation direction. Placing and determining suitable parameters of the second magnet is more challenging than in the first one.

The second magnet is needed to bend the particle trajectories in the other direction with respect to the bend in the first magnet (the opposite magnetic field), such that the beam is also collimated. This means that the geometry of the second sector magnet has to be different. Nevertheless, this is very convenient, because it is not desirable that the beam enters the second sector magnet perpendicularly to its edge. If this happens the size of the beam remains the same without any elongation of slower particles trajectories.

Therefore, the beam has to enter magnet at some angle as shown in Fig. 6.3. Of course, to direct the beam back to initial direction, it has to be bent by the same angle as by the first sector.

The angle of the sector magnet can be determined by basic trigonometry (using the hard edge model again). From Fig. 6.3 the sector length for each particle is

$$v_{1,2} = R_{1,2} \sin \alpha \tag{6.6}$$

the length between sectors e is

$$e = h - v_1 \cot \alpha - v_2 \tan \alpha, \tag{6.7}$$

where h is defined as

$$h = \frac{R_1 + D}{\cos \alpha}. \tag{6.8}$$

Then the sector magnet angle can be rewritten as

$$\tan \Theta = \frac{v_1 - v_2}{e} = \frac{R_1 - R_2}{2} \frac{\sin 2\alpha}{R_1 + D - R_1 \cos^2 \alpha - R_2 \sin^2 \alpha}. \tag{6.9}$$

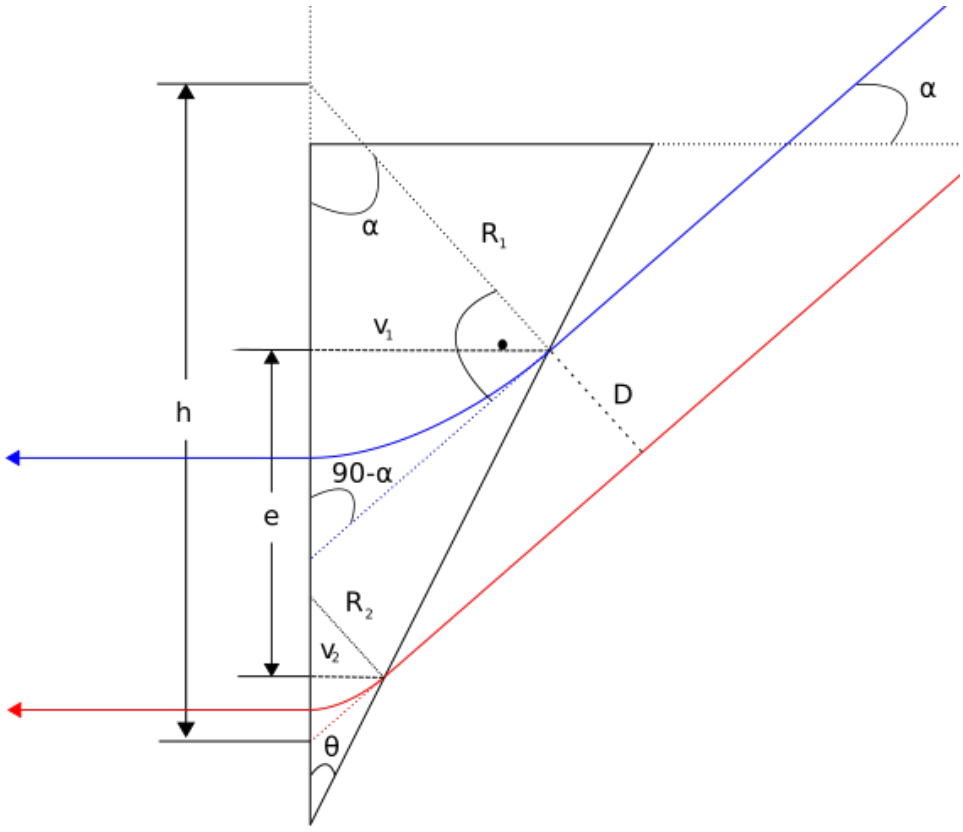

Figure 6.3: The beam propagation through the second sector. The beam direction is angled towards the sector magnet by α. The high energy (blue) and the low energy (red) particle trajectories are curved in the sector magnet by curvature radii R_1 and R_2 with sector lengths v_1 and v_2, respectively. The length between sectors is e. The sector angle is Θ.

The only free parameter here is the magnitude of the magnetic field. Hence this brings two possibilities. Either the magnetic field can be chosen arbitrary and the sector angle calculated from it or the other way around. Nonetheless, a condition $\Theta < \alpha$ must be fulfilled, otherwise the beam cannot be accepted by the second sector magnet (at least at hard edge approximation).

Another condition is the position of the magnet with respect to the beam. The lowest energy particle must enter the magnet (taking y as the vertical coordinate in Fig. 6.3) at

$$y = v_2 \cot \Theta. \tag{6.10}$$

Furthermore, the increased size D_2 of the beam is

$$D_2 = h - R_1 - R_2 \left(1 - \frac{1}{\cos \alpha}\right) \tag{6.11}$$

The scheme of the complete magnetic sector chicane is shown in Fig. 6.4. In this arrangement two middle magnets are united together to form a single magnet, which curve the beam trajectory to a vertically flipped direction. The unification of these magnets is provided because there is no reason to incorporate the drift space in this region. Moreover it decreases the influence of edge effects.

The scheme shows, that the compression magnitutde is scaled with the beam size expansion (similarly to dipole magnetic chicane). Therefore, the compression is increased by an expansion of the angle of one sector magnet or even both of them.

6.2.3 Path difference

The path difference between fastest and slowest particles after sector magnetic chicane can be calculated easily. The difference occurs in magnets and in the drift space between them. For simplicity we do not count in the drift space, which both particles have in common.

The first particle trajectory in all magnets is

$$l_1 = \frac{2\pi\alpha}{180} (\rho_1 + R_1) \tag{6.12}$$

and for the second one

$$l_2 = \frac{2\pi\alpha}{180} (\rho_2 + R_2) + [(R_1 + D) \tan \alpha - R_2 \tan \alpha]. \tag{6.13}$$

Consequently, the path difference caused by sector magnetic chicane is

$$\Delta l = \frac{2\pi\alpha}{180} (\rho_2 + R_2 - \rho_1 - R_1) + (R_2 + D - R_1) \tan \alpha. \tag{6.14}$$

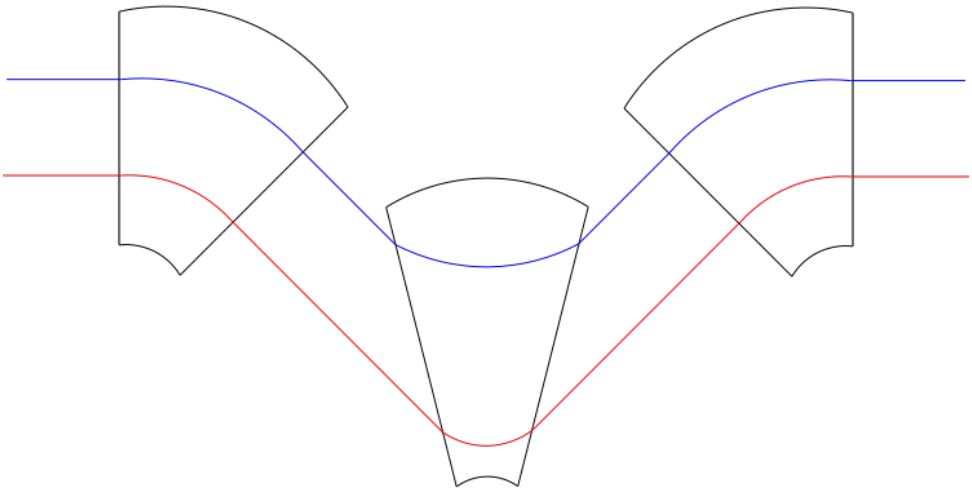

Figure 6.4: Magnetic sector chicane scheme. The beam (blue and red lines) direction is angled by the first sextor magnet towards the second sector, where its size is extended and, subsequently, reduced to the inital one. Then the beam is bent towards the third sector, which angles it to the initial direction

6.3 Enhanced focusing system design

To complete a final achromatic, isochroneous focusing system we suggest to combine dipole to reverse the beam, sector magnetic chicane as compressor and two quadrupoles with one sextupole for achromatic focusation. Since a longitudinal (time) compression of the beam is also provided by the quadrupole and the sextupole focusation, there are two possibilities to operate the whole system.

One option is to slightly overcompensate the particle trajectories by the magnetic chicane, such that the slowest particles will be at the end of the bunch. Then the compression is provided by sending the lowest energy electrons to the centre of the focusing system (as performed in Sec. 5.4). However, this method requires very precise computation of the path difference between fastest and slowest electrons in both magnetic chicane and focusing multipole magnets, which would be very difficult. More gentle adjustment would be possible only by shortening a space between each part of the whole focusing system, which is limited and would not be sufficient for high energy beams.

Another option is to undercompensate the beam and subsequently point the fastest particles to the centre of magnets in focusing system. This method has an advantage, because compression can be gently adjusted by changing the drift space length (especially in ultra-relativistic regime, where TOF is a linear function of the energy), which is much easier to compute. Therefore, the

compression by the chicane and focusing system does not have to compensate the whole path difference created by turning the beam. The TOF difference can be measured in the focal spot and then easily calculate the corresponding length of the drift space to add into system. The drift space can be enlarged by changing the position of the dipole or the quadrupoles and sextupole.

Hence, the second option is chosen for our focusing system. The final scheme is shown in Fig. 6.5.

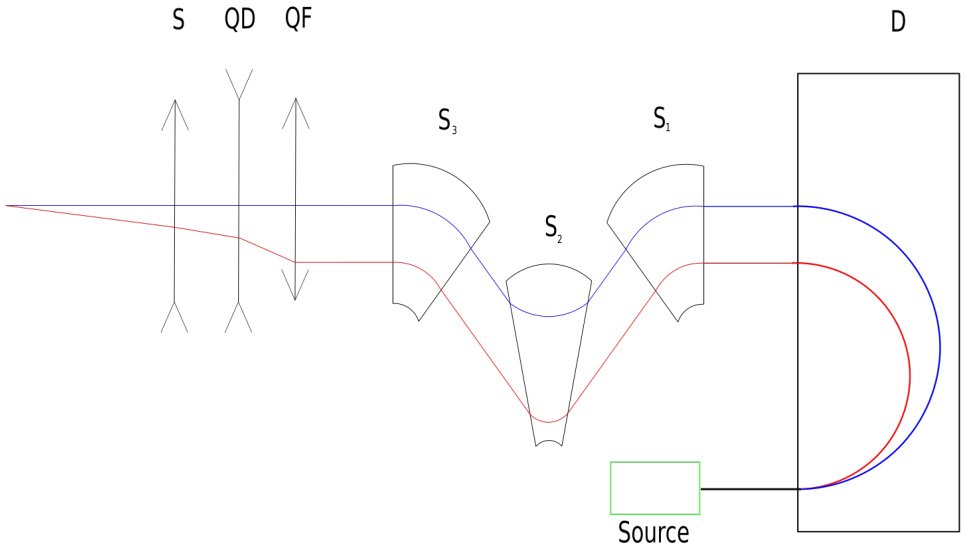

Figure 6.5: Scheme of the final focusing system. Firstly, the beam is reversed by dipole magnet **D** and spatialy chirped by energies: high energy (blue), low energy (red). Subsequently, it is compressed by magnetic chicane consisting of three sector magnets $\mathbf{S}_1$, $\mathbf{S}_2$ and $\mathbf{S}_3$. Finally, the beam is focused by focusing **QF** quadrupole, defocusing **QD** and sextupole **S** magnets.

6.4 Simulation

In this section we show a simulation, which is also performed in SIMION software. However in SIMION we cannot use high magnetic fields and high particle energies simultaneously, due to the large numerical errors occuring during the simulation run. Therefore, the beam energy has to be lowered and later scaling has to be employed to obtain magnetic fields for higher energy.

Since at this point we are more interested into time compression, we use a point like source of the electrons for the simplicity. The input parameters are following. The source position is 32 mm before the front edge of the dipole magnet. The energy of electrons used in simulation is from 3 MeV to 3.5 MeV with a uniform distribution. The magnetic field of the dipole magnet is 290 mT. The angle of the first and third sector magnet is 53 degree.

Their magnetic fields are 145 mT and 124 mT, respectively. The half angle of the second sector magnet is approximately 15.5 degree with the magnetic strength of 231 mT. The field strengths of the focusing, defocusing quadrupoles and sextupole (in the quadrupole approx.) are 1.532 T/m, 1.165 T/m and 1.176 T/m, respectively. The drift space between the quadrupoles is 47 cm and between the quadrupole and the sextupole is 24 mm.

To preserve a longitudinal compression as linear as possible, it is desirable to put focusing magnets closer to each other and use smaller magnetic fields, which will increase the focal length. If this is applied the particle trajectories in each energy line are smoother. Of course, when the low energy beams are used, it is better to keep focal spot close to prevent nonlinearity created by the drift space compression.

Firstly, the time of flight dependence on energy before particles reach the magnetic chicane is shown in Fig. 6.6. The relation is linear as expected and the bunch length is around 60 ps. In Fig. 6.7 we show the TOF energy distribution in the focal spot, which is placed 1828 mm from the front edge of the dipole magnet. As can be seen the beam is compressed to approximately 8 ps, which means that the beam has to be expanded more in the magnetic chicane (sectors with a larger angle should be used).

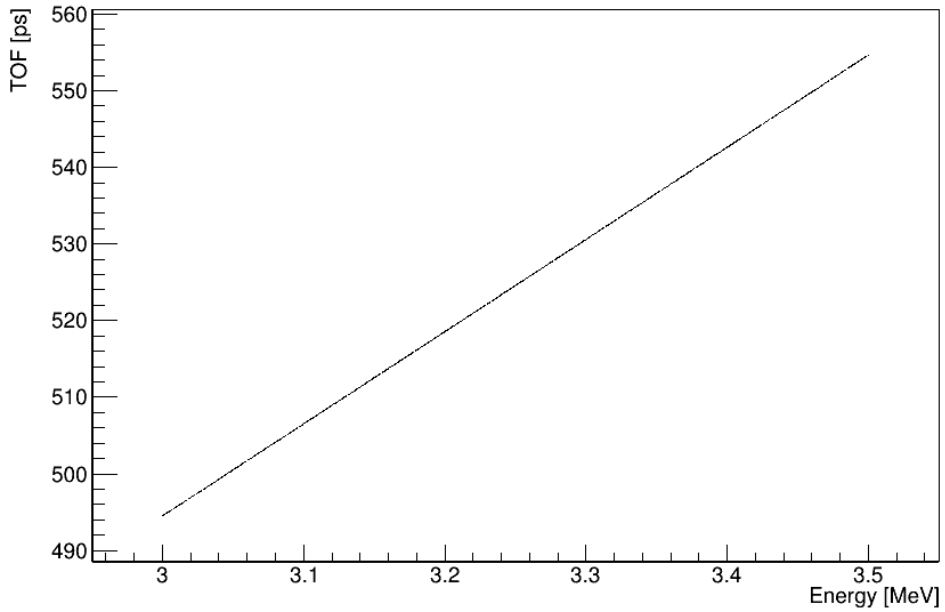

Figure 6.6: TOF energy dependence in position before electrons enter magnetic chicane.

However, the most important result is that the TOF energy relation is more or less linear with the exception of the middle part, but this is due to a beam compression in the drift space. This nonlinearity would disappear, when higher energy beams are used. Therefore, if the low energy beams are focused, the space among the dipole, the chicane and the focusing system

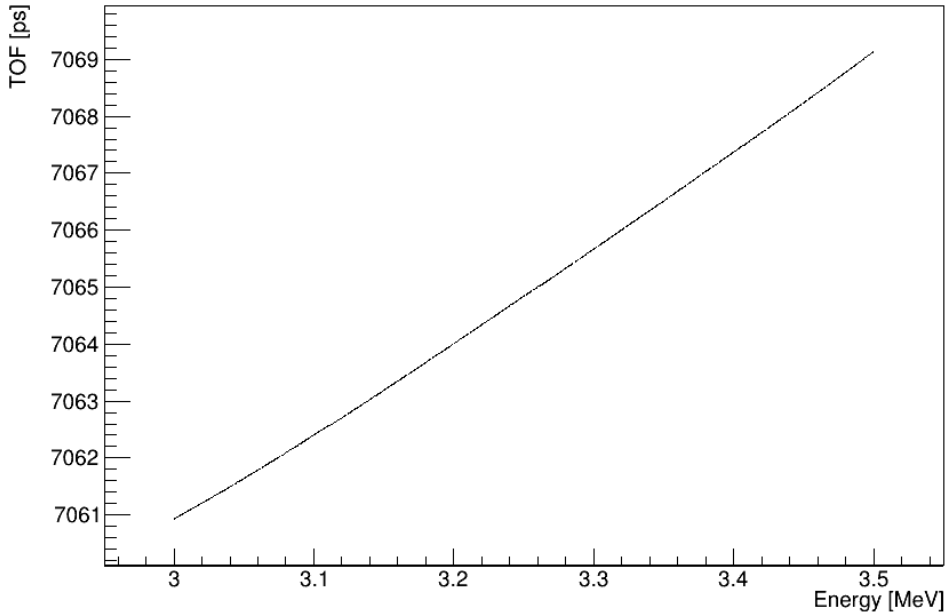

Figure 6.7: TOF energy dependence in focal spot.

should be kept as small as possible. The linear TOF energy dependence in the focus means, that the proposed sector magnetic chicane and focusing system compress the electron beam linearly.

As mentinoned earlier, sector magnets with larger angles are needed for larger compression in our simulation. However, it is very difficult to set magnetic chicane correctly in SIMION. One reason is that sector magnet edge effects are counted in. The other is that the sector represented by SIMION edge is not smooth which leads to more nonlinearities in magnetic fields. Hence, slightly different values of sector magnets than those expected from relations determined in previous section must be applied. For example, the magnetic field of the first and third magnet should be the same. This means that perfectly collimated beam could not be obtained after propagation through the magnetic chicane.

Finally, we show the result of the compression using the drift space expansion. The drift space length is increased by 97 cm. Graph of TOF energy dependence is in Fig. 6.8. The distriubtion is not smooth due to limited precision of TOF determination by SIMION. The beam is now compressed to around 600 fs with U-profile ditribution, which is once again due to "low" energy beam.

6.4.1 Scaling to higher energies

Scaling to higher energies is provided mainly by relation (2.4). However, the beam reversing is limited by the magnetic field used in commonly used magnets. If we want to stick to the same beam radius as performed in the

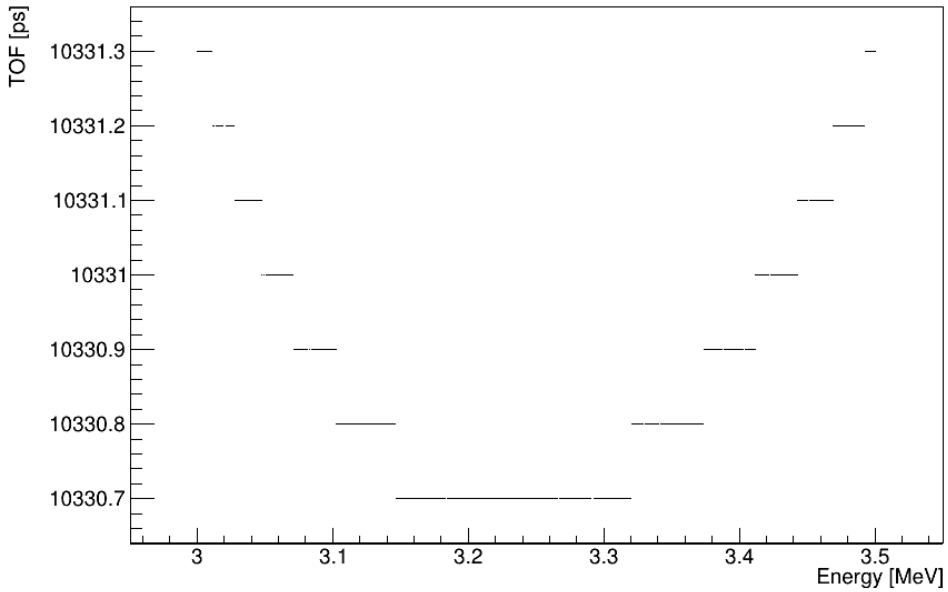

Figure 6.8: TOF energy dependence in focus when compression by drift lngth is applied.

previous section, very large magnetic fields are required. Therefore, the beam size after the reverse has to be enlarged for the high energy beam. Hence, for scaling we have to use results from both simulations in Sec. 5.3.2 and Sec. 6.4.

Consider 100 MeV electron beam with 5% energy spread. If 1.5 T dipole magnet is used, the beam size at the exit is 44 mm. This diameter is even larger than that used in Sec. 5.3.2. Thus, the new sextupole field correction has to be find for this beam size. To get a longer focal length and smoother trajectories, we lowered quadrupoles magnetic fields to 3.1 T/m and 3.7 T/m for focusing and defocusing quadrupole, respectively. The sextupole field strength (quad. approx.) is determined to 1.14 T/m. Focal length is 2 m (measured from the first quadrupole). Distances between magnets are the same as in Sec. 5.3.2. TOF difference in focus between 27 MeV and 30 MeV particle is 3.2 ps.

When the beam has higher energies only magnetic fields are scaled. Other parameters should remain the same. Using (2.4) the quadrupole field strengths scaled to 95-100 MeV beam are 10.5 T/m and 12.7 T/m, respectively and sextupole field strength is 3.9 T/m.

Using (6.3) the TOF difference after the beam reverse is 233 ps. In space 230 ps corresponds to 69 mm. Therefore, the magnetic chicane path difference should be a little less than 69 mm. The rest can be compensated by the drift space.

The first sector magnet should have a magnetic field of 0.75 T; because the angle can be chosen arbitrary, we choose $\alpha = 60$ degree. The magnetic field of the second sector can be determined from (6.14). From this relation we can

evaluate $R_1 - R_2$ by which the magnetic field can be easily computed. If the path difference $\Delta l = 68\,\text{mm}$ is applied, the designated magnetic field of the second sector magnet is 321 mT. The sector half angle is then $\Theta = 30\,\text{degree}$. However, another simulation using a larger beam size is needed to optimize these parameters and determine the additional drift length.

6.4.2 Acceptance

Acceptance of the whole system is mostly limited by focusing system and magnetic chicane. For the layout described in Sec. 5.3.2, electrons with less than 25 MeV could not be focused because of crossing trajectories.

Similarly, if less energetic particles are used in the magnetic chicane, the TOF energy distribution is distorted. Higher energetic particles are accepted (up to 4 MeV), however, the beam is getting slightly divergent with the higher energies after the propagation in the magnetic chicane, but this might be caused by not ideal optimization.

Hence, the acceptance of our focusing system should be more than 10 % of the beam energy, which was performed in both simulations.

Chapter 7

Conclusion

The aim of this work was to propose the achromatic, isochronous focusing system for focusation of the electron beams generated by LWFA having usually finite relative spread (10%). The electron beam energy for which the system was optimized was set to correspond to the energy of electron beams accelerated in the Ti:Sapphire laboratory in PALS research centre.

For the fundamental study and to obtain the basic picture of the focusing system design, the thin lens approximation was used.The beam energy used in Matlab simulation varied from 60 MeV to 110 MeV. The magnetic strength of the sextupole field for chromaticity correction in this approximation was determined (Fig. 3.4).

The simulation performed in SIMION software was applied to study the electron beam spatial chirp by two dipole magnets. To spatially chirp the electron beam to 10 cm diameter with the beam energy from 20 MeV to 40 MeV and the initial diameter 5 mm, the distance between dipole magnets with magnetic field 0.2 T and length 17.5 cm was determined to 13.5 cm.

The design of the electron beam achromatic focusing system consisting of two dipoles, two quadrupoles and the sextupole was proposed. Using SIMION simulation the magnetic field strength of the sextupole magnet was determined to focus the electron beam with the energy from 25 MeV to 35 MeV. The reached focal spot size in the axis, which is transversal to the beam propagation direction, was approximately 1 mm.

The final scheme of the achromatic, isochronous focusing system was suggested. This system contains the dipole magnet, the sector magnetic chciane, two quadrupoles and the sextupole magnet. The simulation was performed to compress the electron beam with the energy from 3 MeV to 3.5 MeV, , due to the necessity od the scaling-down the electron energies owing to the large numerical errors arising in SIMION, to approximately 600 fs on the distance of 2.7 m. The scaling-up of parameters, to the real situation, for focusation of energy from 95 MeV to 105 MeV was determined. The acceptance of the focusing system was estimated to 10 % of the beam energy. The larger compression is possible if the sector magnets with the larger sector angle are used in magnetic chicane. However, for a certain applications, such as fast ignition fusion, the beam duration of 600 fs is sufficient.

Bibliography

[1] T. Tajima, and J. M. Dawson: Laser electron accelerator, Phy. Rev. Lett. **43** (1979) 267.

[2] E. Esarey, C.B. Schroeder, and W. P. Leemans: Physics of laser-driven plasma-based electron accelerators, Rev. Mod. Phys. **81** (2009) 1229.

[3] E. Esarey and M. Pilloff: Trapping and acceleration in nonlinear plasma waves, Phys. Plasmas **2** (1995) 1432.

[4] W. Leemans, E. Esarey, et. al.: Laser guiding for GeV laser-plasma accelerators, Philos. Trans. R. Soc. A **364** (2006) 585.

[5] P. Sprangle, C.-M. Tang and E. Esarey: Relativistic Self-Focusing of Short-Pulse Radiation, IEEE Trans. Plasma Sci. **PS-15** (1987) 145. Beams in Plasmas.

[6] S. Bulanov, et. al.: Particle injection into the wave acceleration phase due to nonlinear wake wave breaking, Phys. Rev. E **58** (1998) R5257.

[7] H. Suk, H. J. Lee, and I. S. Ko: Generation of high-energy electrons by a femtosecond terawatt laser propagating through a sharp downward density transition, Journal of the Optical Society of America B21 (2004) 1391.

[8] D Umstadter, J. Kim, and E. Dodd: Phys. Rev. Lett. **76** (1996) 2073.

[9] V. Horny et al, Short electron bunches generated by perpendicularly crossing laser pulses, Phys. Plasmas 24 (2017) 103125.

[10] H. Wiedemann: Particle accelerator physics, Springer, 2007, ISBN 3 540 49043 2.